PLOS BIOLOGY

RESEARCH ARTICLE

Tooth morphology elucidates shark evolution across the end-Cretaceous mass extinction

Mohamad Bazzi [1]*, **Nicolás E. Campione** [2], **Per E. Ahlberg** [1], **Henning Blom** [1], **Benjamin P. Kear** [3]*

1 Subdepartment of Evolution and Development, Department of Organismal Biology, Uppsala University, Uppsala, Sweden, 2 Palaeoscience Research Centre, School of Environmental and Rural Science, University of New England, Armidale, New South Wales, Australia, 3 Museum of Evolution, Uppsala University, Uppsala, Sweden

* mohamad.bazzi@ebc.uu.se, mohamad_bazzi@hotmail.com (MB); benjamin.kear@em.uu.se (BPK)

Abstract

Sharks (Selachimorpha) are iconic marine predators that have survived multiple mass extinctions over geologic time. Their prolific fossil record is represented mainly by isolated shed teeth, which provide the basis for reconstructing deep time diversity changes affecting different selachimorph clades. By contrast, corresponding shifts in shark ecology, as measured through morphological disparity, have received comparatively limited analytical attention. Here, we use a geometric morphometric approach to comprehensively examine tooth morphologies in multiple shark lineages traversing the catastrophic end-Cretaceous mass extinction—this event terminated the Mesozoic Era 66 million years ago. Our results show that selachimorphs maintained virtually static levels of dental disparity in most of their constituent clades across the Cretaceous–Paleogene interval. Nevertheless, selective extinctions did impact apex predator species characterized by triangular blade-like teeth. This is particularly evident among lamniforms, which included the dominant Cretaceous anacoracids. Conversely, other groups, such as carcharhiniforms and orectolobiforms, experienced disparity modifications, while heterodontiforms, hexanchiforms, squaliforms, squatiniforms, and †synechodontiforms were not overtly affected. Finally, while some lamniform lineages disappeared, others underwent postextinction disparity increases, especially odontaspidids, which are typified by narrow-cusped teeth adapted for feeding on fishes. Notably, this increase coincides with the early Paleogene radiation of teleosts as a possible prey source, and the geographic relocation of disparity sampling "hotspots," perhaps indicating a regionally disjunct extinction recovery. Ultimately, our study reveals a complex morphological response to the end-Cretaceous mass extinction and highlights an event that influenced the evolution of modern sharks.

Introduction

Fossils provide the only direct evidence of interplay between organisms and their environments over vast evolutionary timescales [1–3]. They are, therefore, crucial for exploring the drivers of past biodiversity change and can shed light on the origins of modern ecosystems [3].

However, the analytical challenge is to discern a genuine biological signal from the combined obfuscations of geologic, taphonomic, sampling, taxonomic, analytical, and interpretive biases [4–7]. While these may be impossible to overcome in entirety, the fossil records of some widely distributed and chronostratigraphically extended clades provide exceptional opportunities to characterize macroevolutionary processes through deep time.

Sharks constitute one such group because their dental remains are abundant in Mesozoic and Cenozoic marine deposits—a timeframe covering approximately 250 million years (Ma) [8,9]. Extant shark species are also ecologically disparate, encompassing a spectrum of macrophagous to microphagous predators that account for nearly half (42%) of all the currently documented chondrichthyan biodiversity (N = 1,193 species) [10,11]. Nevertheless, the various biological and environmental factors that have shaped shark evolution remain obscure. In particular, their capacity to survive mass extinctions is relevant for understanding the dramatic decline of shark populations observed in our modern oceans [11–16].

The end-Cretaceous mass extinction (approximately 66 Ma), which marks the Cretaceous/ Paleogene (K/Pg) chronostratigraphic boundary, is especially pertinent because it profoundly disrupted marine ecosystems but has disputed implications for shark species diversity and morphological disparity. Indeed, contrasting interpretations advocate either limited [17] or complex interrelationships of biotic and abiotic drivers that seemingly influenced shark evolution from before, during, and after the K/Pg mass extinction event [18–21]. Here, we explore these contentions via a comprehensive assessment of shark dental morphology across the end-Cretaceous mass extinction. Our study expands on previous studies that targeted either geographically localized [22,23] or clade-specific [21] assemblages. We use a dataset of 1,239 fossil shark teeth, representing 9 major selachimorph clades sampled at global and regional scales. These groups include the following: the Galeomorphii orders Carcharhiniformes, Heterodontiformes, Lamniformes, Orectolobiformes; the Squalomorphii orders Echinorhiniformes, Hexanchiformes, Squaliformes, Squatiniformes; and the extinct [†] Synechodontiformes. Our approach uses geometric morphometrics to compare disparity and morphospace patterns across a constrained 27.6-million-year interval spanning the Campanian and Maastrichtian ages of the Late Cretaceous (83.6 to 66 Ma) to the Danian, Selandian, and Thanetian ages (= Paleocene epoch) of the early Paleogene (66 to 56 Ma). We test the following hypotheses that: (1) selachimorph disparity was in decline before marine ecosystem disruption during the end-Cretaceous mass extinction, resulting from major marine transgressions during the Maastrichtian [23,24]; (2) selachimorph taxonomic richness depletion at the K/Pg boundary [18,19] was coupled with eco-morphological turnover; (3) apex predator shark lineages were disproportionately impacted, consistent with similar losses in marine tetrapods and osteichthyans [18,21,25]; and (4) extinction and recovery patterns were consistent at global and regional scales [21–23].

Materials and methods

Dataset assembly

Our dataset was compiled using photographs and graphic images derived from first-hand observations or the literature (S1 Data, Fig A and Tables A and B in S1 Text). Following recommended best practices [21,26,27], we screened the raw image data to include only those depicting complete tooth crowns with adequate resolution to determine the crown–root junction. The global sampling includes nearly all major selachimorph orders (Fig A in S1 Text, Fig B in S1 Text, panel A), except for Pristiophoriformes (Sawsharks), which are sparsely documented [8,28]. We also elevated Echinorhinidae to Echinorhiniformes [29–31] and employed a sensitivity analysis to test the morphospace occupation and disparity effects of

†Synechodontiformes, which has been classified as either a clade within Galeomorphii or a neoselachian sister lineage (Fig B in S1 Text, panel A) [32–35]. Finally, most images were captured in the labial aspect, unless only a lingual view was available, and with the tooth apex directed to the left (Fig C in S1 Text). The equivalency of labial and lingual views [21] was tested using ordinary least-squares linear models based on a subsample of the labial and lingual view data (N = 866).

Time-binning encompassed 5 geochronological ages spanning the immediate K/Pg interval: Campanian and Maastrichtian/Danian, Selandian, and Thanetian. However, we also implemented an alternative 4-age time-binning scheme that pooled temporally ambiguous specimens assigned to the Danian and Selandian (Tables C and D in S1 Text). In addition, we carried out analyses using a subsample of the dataset (N = 659) for which "early" and "late" sub-ages could be defined for the Campanian and Maastrichtian and "early," "middle," and "late" for the Danian (Table E in S1 Text). Numerical age values, in Ma, were taken from the International Chronostratigraphic Chart v2020/03 [36] and used as references for plotting.

Acquisition of geometric shape data

Landmark-based geometric morphometrics quantifies biological shapes as a series of evolutionary homologous points in Cartesian space [26,27,37–42]. However, evolutionary homology [37,38] between landmarks cannot be assumed because of the inherent morphological variability in shark teeth (e.g., the location and number of cusplets). As a result, we designated our landmark placements based on topological rather than evolutionary homology [41].

Landmark digitization was carried out in *tpsDig2* v. 2.31 [43] with resampling to a standard number of equidistant semilandmarks using customized code in *R* v. 4.0.5 [44]. The resulting scheme comprised 2 open curves defined by semilandmarks but anchored by 3 fixed landmarks: Type 1 landmarks delimited the mesial and distal crown–root junctions, and a Type 2 landmark pinpointed the tooth apex (sensu [37]; Fig B in S1 Text, panel B, Table F in S1 Text). The number of semilandmarks (k) was determined using resampling of the mesial and distal curves at equal spacings of k = 40, 60, 80, 100, 120, 140, and 160. Qualitative observations (Figs D and E in S1 Text) found that k = 160 best-captured tooth shape complexity and included distal and mesial curves of 78 and 79 sliding semilandmarks, respectively. Tooth serrations were not digitized because of limited image resolution, but we acknowledge that these structures are functionally important [45].

Lastly, to screen for possible digitization errors, we extracted a random subsample of 30 tooth images (Table G in S1 Text) and used a one-way ANOVA to calculate the intraclass correlation coefficient (*R*) [26,46,47] (also see S1 Text). We also ran a 2-block partial least-squares (2B-PLS) analysis to infer covariation between the landmark datasets. Other exploratory procedures were employed to assess measurement error: (1) a manual survey of digitized images to confirm landmark placement accuracy; (2) screening of outliers visualized in the morphospace plots and associated thin plate spline (TPS) deformation grids, as well as being identified using the *plotOutliers* search function in *geomorph* v. 4.0.0 [48].

Morphometric analysis

To standardize our digitized specimens for unit size, position, and rotation, we used a generalized Procrustes analysis (GPA) [49,50] that minimizes the bending energies to optimize the positions of the sliding semilandmarks [50,51]. Because large numbers of semilandmarks can impinge on GPA convergence [26,38], we varied the iteration frequency by arbitrarily increasing the *max.iter* argument in *gpagen* to compare convergence criteria Q-values (= Procrustes

sum of squares). The resulting consensus shape configurations were then inspected (Fig F and Table H in S1 Text).

The aligned Procrustes coordinates were ordinated via a principal components analysis (PCA) based on the singular value decomposition of the variance–covariance matrix. Shape variation was depicted as both TPS deformation grids and deformation isolines to generate a concentration "heat map" [52]. Morphospace was visualized using back-transformation [53,54]. All analyses were carried out in *R* v. 4.0.5 [44] with the *geomorph* v. 4.0.0 [48] and *RRPP* v. 1.0.0 [55] packages; visualization used the *ggplot2* package [56]. All data and *R* scripts are available from *Data Dryad* under DOI: https://doi.org/10.5061/dryad.c866t1g5n [57].

Temporal analyses of morphospace

Morphospace was depicted as time-bin box plots that incorporate the arithmetic mean, median, and modal values. Confidence intervals were calculated using nonparametric bootstrapping with 1,000 resamples. Comparisons between multiple central tendency values accommodate for differences in frequency distributions. Modal shape configurations correspond to the region of maximum frequency calculated as:

$$Mo_{shape_j} = \hat{\mu}_p + Mo_{C_j} \times \Gamma_j \tag{1}$$

where Mo_{shape_j} is the modal shape configuration of the *j*th PC; $\hat{\mu}_p$ represents the mean shape configuration of the whole sample; Mo_{C_j} is the mode of the *j*th PC axis; and, Γ_j is the rotation matrix corresponding to the *j*th PC. Mo_{shape_j}, $\hat{\mu}_p$ and Γ_j take the form of k × m matrices and were plotted as TPS deformation grids; "k" is the number of landmarks and "m" is the dimensions, in our case two.

Multivariate normality was assessed using a Henze–Zirkler test [58] ($HZ = 4,956$, $p = 0$) (Fig G in S1 Text). Statistical comparisons between time-bins used a nonparametric Procrustes analysis of variance implemented in the *RRPP* package [55].

Temporal analyses of disparity

We calculated Procrustes variance (PV) as a measure of disparity [41,59] based on the 2D (k × m × N) Procrustes-aligned landmark dataset:

$$SSW_n = (x_1 - \bar{x}_1)^2 + (y_1 - \bar{y}_1)^2 + \cdots + (x_k - \bar{x}_k)^2 + (y_k - \bar{y}_k)^2 \tag{2}$$

where SSW_n is the sum of the square distances between the coordinates (x_k and y_k) of observation *n* and their associated mean ($\bar{x}_k$ and $\bar{y}_k$) [48]. This equation can be alternatively depicted as:

$$SSW_n = \sum_{k=1}^{k} (x_k - \bar{x}_k)^2 + (y_k - \bar{y}_k)^2 \tag{3}$$

All SSW_n values in a given time-bin *t* are then summed and divided by the sample size at that time (N_t) to measure PV across all observations [48]. Note that the following equation was erroneously presented in Bazzi and colleagues [21].

$$PV_t = \frac{\sum_{n=1}^{n} SSW_n}{N_t} \tag{4}$$

Disparity within each time-bin was partitioned according to their taxonomic order-level classifications, which determined the clade-specific contributions to the overall disparity. This

calculation equates to (3), but with distances measured relative to the mean of the group i ($\bar{x}_{k|i}$), rather than the overall mean [48]:

$$SSW_n = \sum_{k=1}^{k} (x_k - \bar{x_{k|l}})^2 + (y_k - \bar{y_{k|l}})^2 \qquad (5)$$

The partial PV for the group i in a specific time-bin t is $\therefore$.

$$PV_{i|t} = \frac{\sum_{n=1}^{n} SSW_n}{n_i} \times \frac{n_i}{N-1} \qquad (6)$$

where n_i is the sample size of group i and N is the total sample size within t [48].

Computationally, these equations are solved in *geomorph* [48], with the expectation that additive partial disparities [60] for sampling within each time-bin approximate the total PV given t.

We used a residual randomization permutation procedure (RRPP) with 1,000 permutations [55] to test null hypotheses for our multivariate shape data as:

$$H_0 : |PV_{t1} - PV_{t2}| = 0$$
$$H_A : |PV_{t1} - PV_{t2}| > 0 \qquad (7)$$

H_0 assumes that pairwise absolute differences between PVs across 2 given time-bins (e.g., *t1* and *t2*) will be zero. H_A alternatively stipulates that the difference will be greater than zero.

We also applied nonparametric bootstrap resampling to estimate confidence intervals around disparity. All post hoc pairwise comparisons of group means were subject to false discovery rate (FDR) adjustments of *p*-values to mitigate the increased risk of Type I errors associated with multiple comparisons [61].

Geographic distribution in the fossil record

We accommodated for sample size biases inherent in the fossil record [4,62–64] via rarefaction comparisons of time-scaled PV [21]. These involved subsampling (999 iterations) of all time-bins to a minimum size (Tables A, C, and D in S1 Text), after which 95% prediction intervals were calculated. Geographic subsampling focused on the UNESCO World Heritage fossil locality at Stevns Klint in Denmark (Fig H in S1 Text), which preserves exceptionally rich selachimorph assemblages [65,66] spanning the K/Pg succession [67]. However, we also calculated partial disparities for each time-bin based on marine depositional basins, designated i in (6). Although the precise boundaries of these basins are ambiguous, they do provide a convenient proxy for comparing regional versus global disparity signals across a broader subsampled series.

Influences of heterodonty

Sharks are known to exhibit both monognathic (variation along the tooth row) and dignathic (variation between the upper and lower jaws) heterodonty [8,68], although this can be difficult to discriminate from isolated fossil teeth [69]. To mitigate, we relied upon established diagnostic criteria [21,70] to categorize our specimens as representing parasymphyseal, anterior, lateroposterior, or posterior tooth positions ($N_{MH} = 897$), and deriving from either the upper or lower tooth rows ($N_{DH} = 334$) (see S1 Text)

$$Shape \sim ToothPosition + t \qquad (8)$$

where the aligned Procrustes coordinates (*shape*) are described as a function of monognathic or dignathic *Tooth Position* at age *t*.

Because developmental [70,71] and ontogenetic factors [70,72–74] also affect selachimorph tooth morphology, our analyses are presented with the caveat that adequate intraspecific coverage was assumed for each order-level clade.

Results

Digitization measurement error

Visual comparison of the computed consensus (mean) tooth shapes (Fig I in S1 Text) indicates consistent digitization across landmark datasets. Accordingly, an intraclass correlation coefficient (*R*) of 2% (or 1 in 50) was calculated based on the aligned Procrustes coordinates and their error replicate counterparts (*N* = 30) (Table I in S1 Text). Pearson product–moment correlation (t = 1,874.7, *df* = 9598, *p*-value $\ll$ 0.001, R = 0.99) and a 2B-PLS test (r-pls = 0.997, *p*-value = 0.001, Z = 7.136) unambiguously demonstrate dataset compatibility (Fig J in S1 Text).

PCA visualization

PC1 to PC4 explain 89.28% of the shape variance (Fig 1A–1C, Fig K in S1 Text), with the remaining PC axes collectively describing 10.71% (Fig K and Table J in S1 Text). PC1 (62%) captures tooth height and width variation from apicobasally tall and narrow teeth to mesiodistally broad and low crowns (Fig L in S1 Text, panel A). PC2 (12%) alternatively represents distally recurved teeth with low "heels" versus upright triangular teeth with lateral cusplets (Fig L in S1 Text, panel B). PC3 (11%) tracks tall and conical to distally wide and recurved teeth with pronounced lateral cusplets (Fig L in S1 Text, panel C). PC4 (5%) depicts a spectrum of short triangular teeth with reduced cusplets to tall crowns with prominent cusplets commensurate in height with the main cusp (Fig L in S1 Text, panel D).

While there is a substantial overlap in tooth morphologies between selachimorph clades (Fig 1A–1C), a general Procrustes one-way ANOVA found significant differences between the group means, both generally and along specific axes of variance (Table 1). Such results are supported by visible segregation between the clades in morphospace (Fig 1A–1C) and are further illustrated by measures of central tendency, distribution symmetries, and normality and multimodality tests (Table K in S1 Text).

Global and regional disparity

We find overall stability in selachimorph global disparity across the Campanian–Thanetian interval (Fig 2, Table L in S1 Text). The only exception was a significant decline within the Selandian time-bin (PV_{Danian} = 0.082; $PV_{Selandian}$ = 0.042; *p* = 0.033), which may be a product of sampling (*N* = 28) and/or uneven clade representation. Disparity during the Thanetian exceeded (Fig 2, Fig M and Table L in S1 Text) that of the preextinction Campanian ($PV_{Campanian}$ = 0.069; $PV_{Thanetian}$ = 0.085; *p* = 0.033) and was unaffected by pruning of †Synechodontiformes as a possible selachimorph stem group (Fig 2, Table M in S1 Text). Comparisons with the Stevns Klint regional subsample found no significant change in tooth disparity ($PV_{lateMaastrichtian}$ = 0.091; $PV_{earlyDanian}$ = 0.069; *p* = 0.106) across the K/Pg boundary (Fig 2, Table N in S1 Text). However, a significant disparity increase occurred after the extinction event from the early to middle Danian ($PV_{earlyDanian}$ = 0.069; $PV_{middleDanian}$ = 0.123; *p* = 0.005).
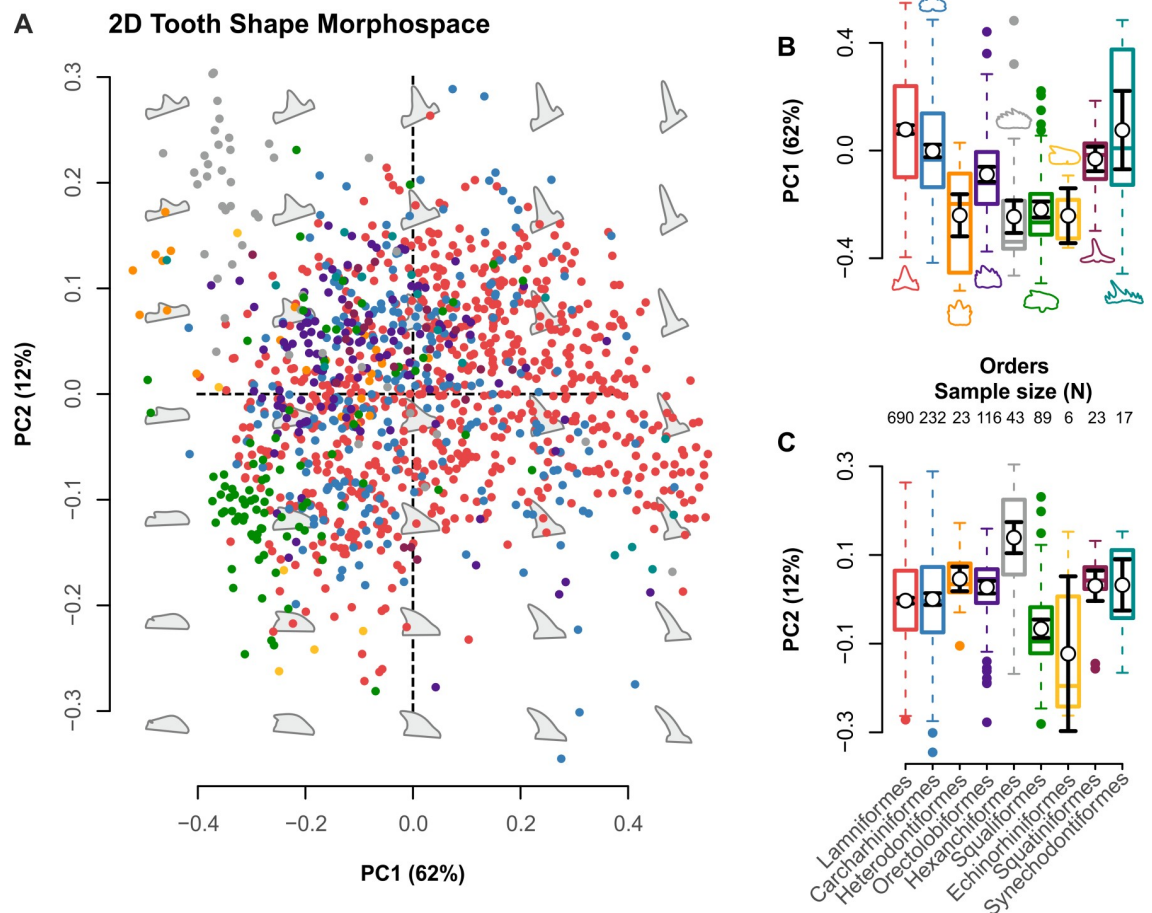
A   2D Tooth Shape Morphospace

Fig 1. Morphospace distribution. (A) Multivariate shape space for the $N = 1,239$ global selachimorph tooth sample. Theoretical backtransform tooth shapes (gray) indicate shape variability across morphospace as defined by PC1/PC2. (B, C) Box-and-whisker plots indicating average morphospace occupation along (B) PC1 and (C) PC2. Error bars represent 95% confidence intervals. Proportion of variance and group sample sizes are listed in the axis labels. The data used in this analysis can be accessed online at https://doi.org/10.5061/dryad.c866t1g5n.

https://doi.org/10.1371/journal.pbio.3001108.g001

Superorder-level clade disparity

Relative stasis characterized the disparity of both galeomorphs and squalomorphs across the Maastrichtian–Danian-Selandian (Fig 3A and 3B, Tables O, P, and Q in S1 Text). This result is consistent even after the exclusion of †synechodontiforms (Fig 3A, Table P in S1 Text). Conversely, independent testing of the Stevns Klint regional subsample produces a significant disparity increase among galeomorphs ($PV_{earlyDanian} = 0.069$; $PV_{middleDanian} = 0.109$; $p = 0.022$) in the early to middle Danian (Fig 3A, Tables R and S in S1 Text) and a corresponding reduction in squalomorph disparity (Fig 3B, Table T in S1 Text) across the late Maastrichtian to early Danian ($PV_{lateMaastrichtian} = 0.077$; $PV_{earlyDanian} = 0.041$; $p = 0.005$).

Order-level clade disparity

Lamniform and carcharhiniform (Fig 4A and 4B, Tables U and V in S1 Text) disparities were highest during the Campanian and Maastrichtian interval (Fig 4A and 4B). Despite these high levels, global lamniform disparity was demonstrably stable across the Maastrichtian–Danian-Selandian time-bins ($PV_{Maastrichtian} = 0.070$; $PV_{Danian-Selandian} = 0.059$; $p = 0.396$; Fig 4A) and

Table 1. Nonparametric analysis of variance based on RRPP for N = 1,239. Coefficient estimation via OLS. Type I (sequential) sums of squares were used to calculate the sums of squares and cross-products matrices. Effect sizes (Z) are based on the F distribution.

	d.f.	SS	MS	R²	F	Z	Pr(>F)
All PC axes							
~ groups (clades)	8	18.744	2.34294	0.18931	35.904	10.892	**0.001****
PC1							
~ groups (clades)	8	13.737	1.71707	0.22474	44.569	7.3642	**0.001****
PC2							
~ groups (clades)	8	1.4895	0.186190	0.12352	21.668	5.8106	**0.001****
PC3							
~ groups (clades)	8	2.1710	0.271372	0.20412	39.431	7.0403	**0.001****
PC4							
~ groups (clades)	8	0.3986	0.049819	0.08708	14.665	5.1632	**0.001****

d.f., degrees of freedom; F statistics, F value by permutation; MS, mean squares; OLS, ordinary least squares; RRPP, residual randomization permutation procedure; R^2, coefficient of determination; SS, sequential sums of squares; Z, effect size.

p-Values are based on 999 permutations.

https://doi.org/10.1371/journal.pbio.3001108.t001

showed no significant change by the Thanetian ($PV_{Maastrichtian} = 0.070$; $PV_{Thanetian} = 0.055$; $p = 0.264$; Fig 4A).

Carcharhiniforms otherwise exhibited a marked disparity decline from the Campanian to Danian-Selandian when using the global sample, but not in the Stevns Klint regional
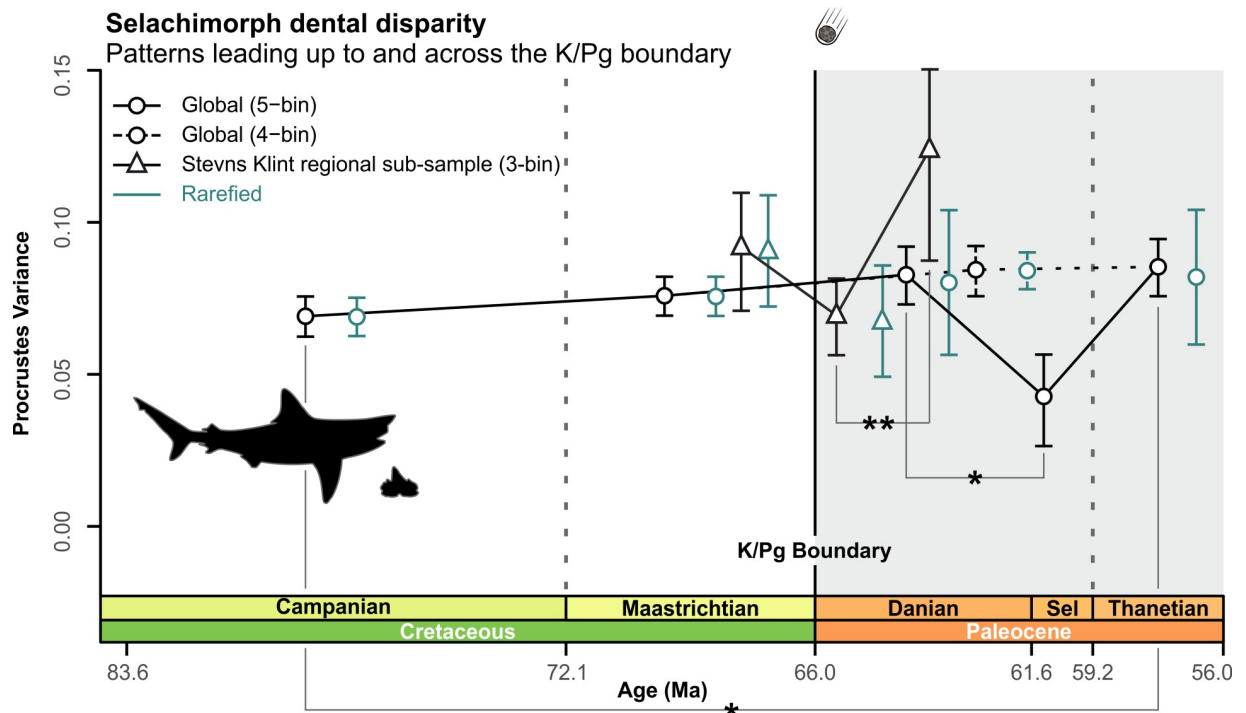

Fig 2. Global and regional level disparity of Selachimorpha. Dental disparity with bootstrapped prediction intervals for the 5- and 4-age time-binning schemes. The 5-age time-binning scheme ($N = 1,156$) utilized sample rarefaction on the lowest sampled Selandian time-bin ($N = 28$). The 4-age time-binning scheme ($N = 1 198$) used the Thanetian ($N = 187$). The Stevns Klint regional subsample (3-age time-bin) used the middle Danian ($N = 25$). Significant FDR-adjusted p-values for multiple comparisons are indicated (*$p < 0.05$, **$p < 0.005$). Silhouette graphics created by MB. The data used in this analysis can be accessed online at https://doi.org/10.5061/dryad.c866t1g5n. FDR, false discovery rate; K/Pg, Cretaceous/Paleogene; Ma, million years; Sel, Selandian.

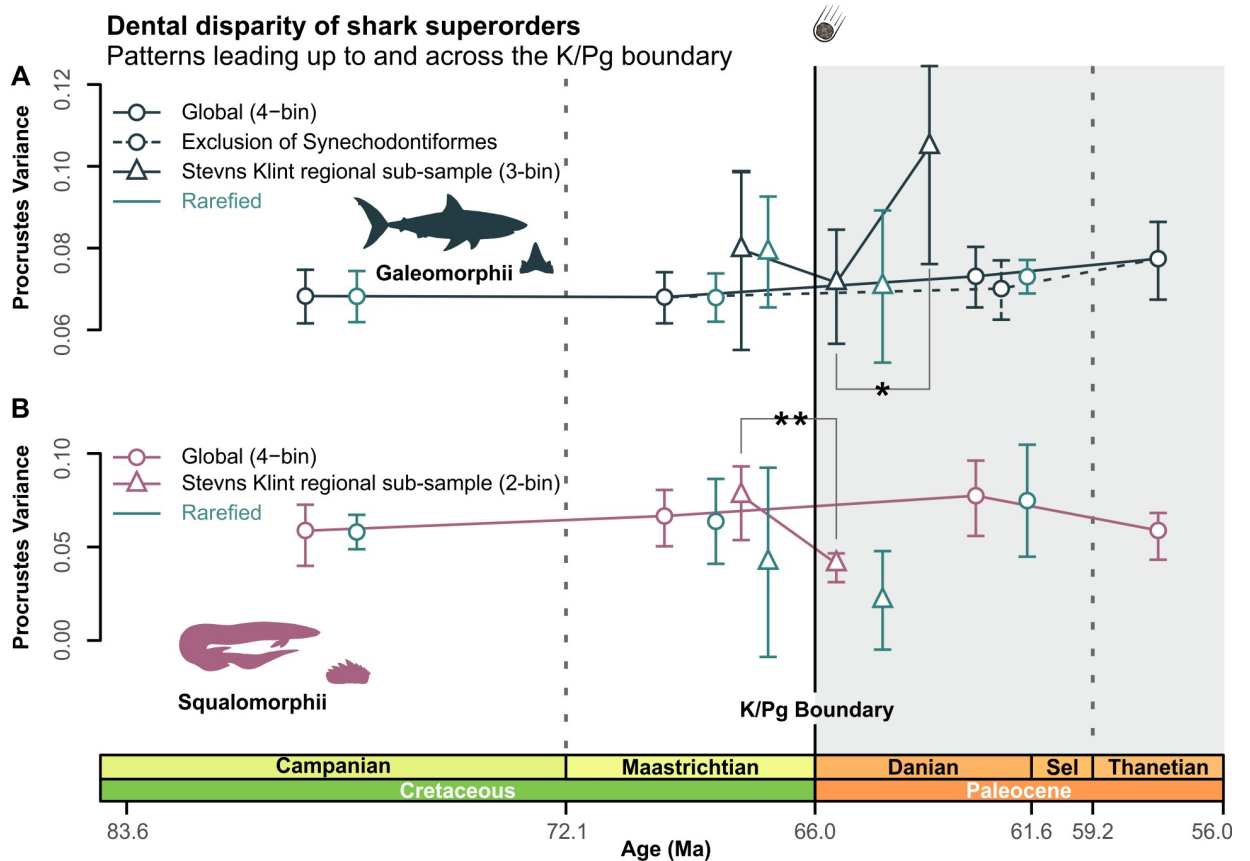https://doi.org/10.1371/journal.pbio.3001108.g002

Fig 3. Superorder-level clade disparity profiles. (A, B) Global/regional raw and rarefied dental disparity trajectories for Galeomorphii (including and excluding †Synechodontiformes) and Squalomorphii. Sample rarefaction: Galeomorphii, $N = 169$; Squalimorphii, $N = 18$. Significant FDR-adjusted p-values for multiple comparisons are indicated ($*p < 0.05$, $**p < 0.005$). Silhouette graphics created by MB. The data used in this analysis can be accessed online at https://doi.org/10.5061/dryad.c866t1g5n. FDR, false discovery rate; K/Pg, Cretaceous/Paleogene; Ma, million years; Sel, Selandian.

https://doi.org/10.1371/journal.pbio.3001108.g003

subsample (Fig 4B, Table V in S1 Text). A distinct disparity drop across the Campanian–Maastrichtian ($PV_{Campanian} = 0.085$; $PV_{Maastrichtian} = 0.056$; $p = 0.024$) was followed by stasis from the Maastrichtian–Danian-Selandian ($PV_{Maastrichtian} = 0.056$; $PV_{Danian-Selandian} = 0.041$; $p = 0.125$) and a subsequent disparity increase by the Thanetian ($PV_{Danian-Selandian} = 0.041$; $PV_{Thanetian} = 0.061$; $p = 0.020$) (Fig 4B).

Heterodontiform disparity was uniform across the Campanian–Thanetian interval (Fig 4C, Table W in S1 Text). On the other hand, orectolobiforms showed a significant disparity increase ($PV_{Campanian} = 0.024$; $PV_{Danian-Selandian} = 0.064$; $p = 0.016$) between the Campanian and Danian-Selandian (Fig 4D, Table X in S1 Text). We recover no significant change in orectolobiform disparity for any time-bin comparisons, including the Maastrichtian–Danian-Selandian ($PV_{Maastrichtian} = 0.041$; $PV_{Danian-Selandian} = 0.064$; $p = 0.096$), which is consistent with the results based on the Stevns Klint regional subsample ($PV_{lateMaastrichtian} = 0.109$; $PV_{earlyDanian} = 0.066$; $p = 0.294$) (Fig 4D).

Hexanchiform disparity was not statistically differentiated across the Maastrichtian–Danian-Selandian ($PV_{Maastrichtian} = 0.018$; $PV_{Danian-Selandian} = 0.124$; $p = 0.104$) nor between the Danian-Selandian and Thanetian ($PV_{Danian-Selandian} = 0.124$; $PV_{Thanetian} = 0.054$; $p = 0.072$) (Fig 4E, Table Y in S1 Text). Squaliforms similarly maintained stable disparity from the Maastrichtian–Danian-Selandian ($PV_{Maastrichtian} = 0.054$; $PV_{Danian-Selandian} = 0.032$; $p = 0.084$), both
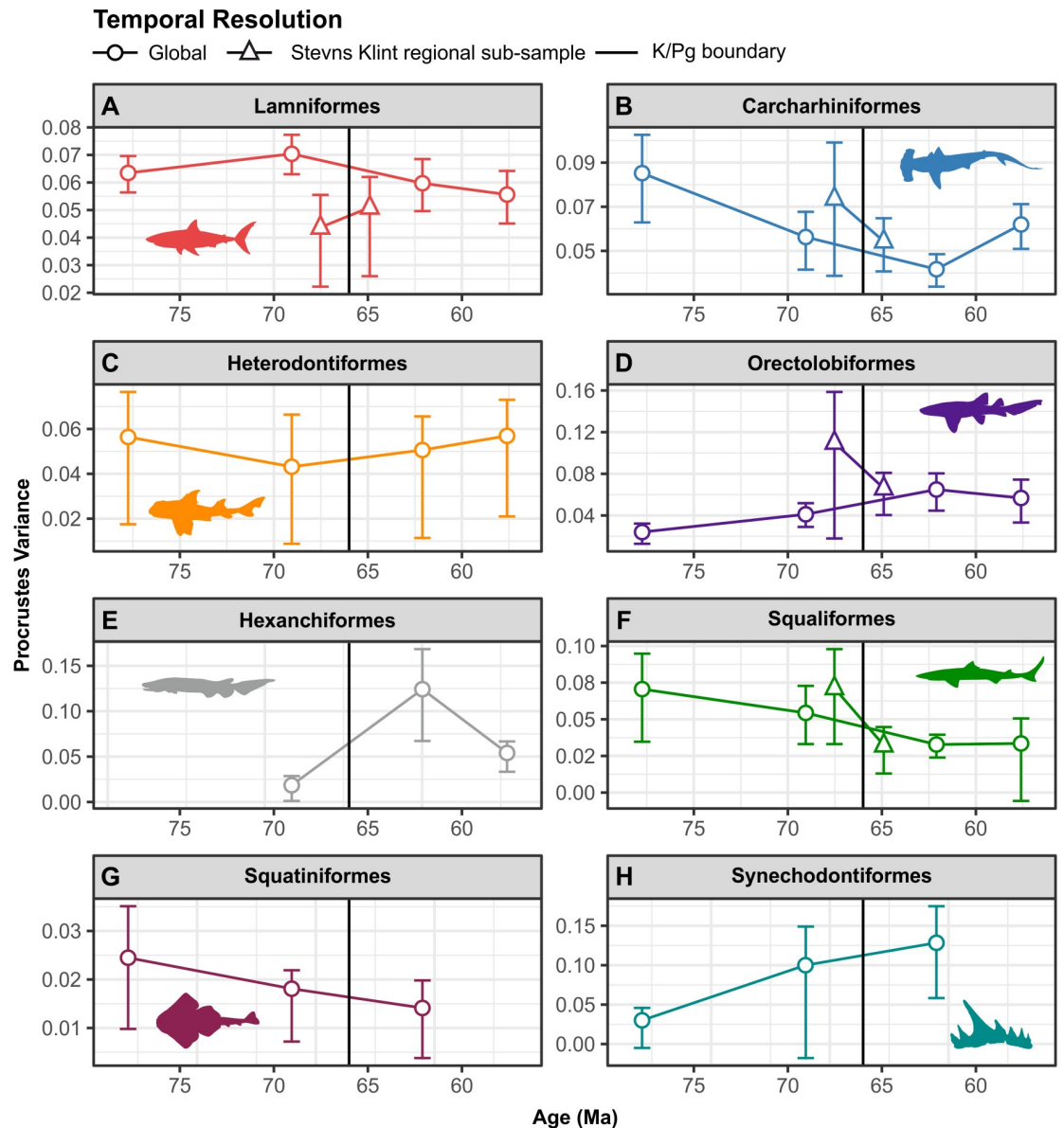
Fig 4. Global and regional clade-specific (order-level) disparity profiles. (A–D) Temporal resolution varies between groups but broadly tracks the time-binned K/Pg interval. Clade-level subsampling is shown in Tables C and D in S1 Text. Silhouette graphics created by MB and Julius Csotonyi (https://csotonyi.com/). The data used in this analysis can be accessed online at https://doi.org/10.5061/dryad.c866t1g5n. K/Pg, Cretaceous/Paleogene; Ma, million years.

https://doi.org/10.1371/journal.pbio.3001108.g004

within the global and Stevns Klint regional samples (Fig 4F, Table Z in S1 Text). Finally, squatiniform and †synechodontiform disparities were also stable, but their small sample sizes make interpretations equivocal (Fig 4G and 4H, Tables AA and BB in S1 Text).

Global partial disparity

PVs indicate that selachimorph global disparity was driven by lamniforms during the Campanian and Maastrichtian (Fig 5A). Unsurprisingly, lamniforms were also the most numerically abundant taxa during this time (Fig A in S1 Text). Lamniform contribution to global disparity
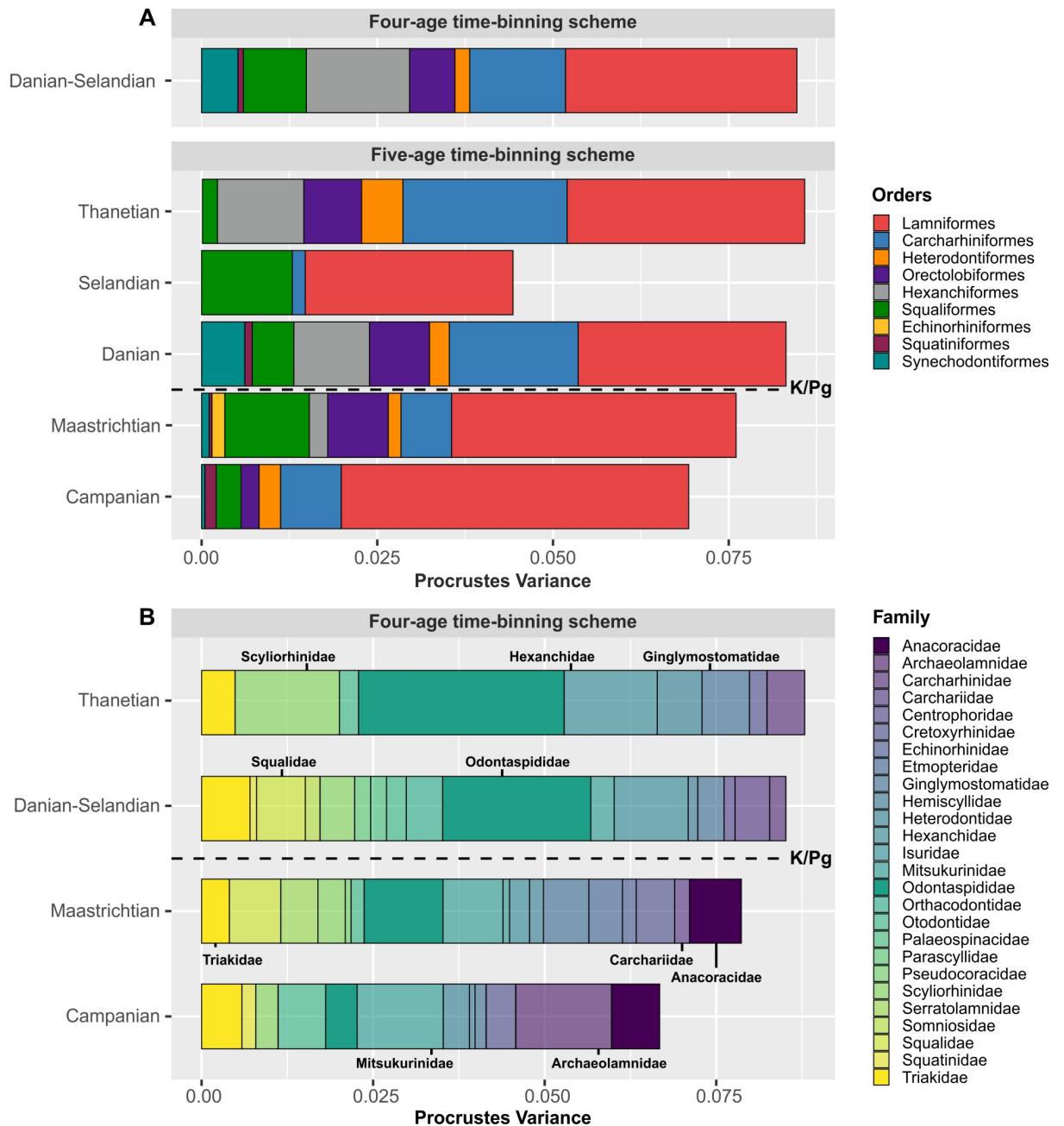
Fig 5. Order- and family-level partial disparity. (A, B) Grouped bar plot depicting clade-level contributions to overall disparity in each time-bin. (B) Families with sample sizes of $N < 5$ were omitted. Resulting data total = 26 families and 1,039 specimens with the global 4-age time-binning scheme. The data used in this analysis can be accessed online at https://doi.org/10.5061/dryad.c866t1g5n.

https://doi.org/10.1371/journal.pbio.3001108.g005

subsequently decreased in the Danian (Fig 5A) but increased again in the Selandian, although the sample size is small (Table C in S1 Text). Overall, lamniforms accounted for almost all of the global selachimorph variance calculated across the K/Pg time interval (Fig 5A). Carcharhiniforms and hexanchiforms otherwise contributed to a global disparity increase from the Danian to the Thanetian (Fig 5A).

Despite uneven sampling, family-level partial disparities (Fig 5B) reveal that archaeolamnids, mitsukurinids, and anacoracids provided the primary sources of selachimorph disparity during the Campanian. Odontaspidids sequentially increased their disparity from the Danian-Selandian to the Thanetian (Fig 5B). Correspondingly, triakids, hexanchids, and squalids contributed markedly to non-lamniform disparity in the Danian-Selandian, with scyliorhinids increasing disparity in the Thanetian. Other clades, such as ginglymostomatids and hexanchids, also increased disparity from the Danian-Selandian–Thanetian (Fig 5B).

Geographic distribution of disparity

Samples from the North American Western Interior (WIB) and European epicontinental (EEB) basins accounted for most of the disparity during the Campanian (Fig 6). Alternatively, the Maastrichtian incorporated a substantial contribution from the Ouled Abdoun and Tarfaya basins (= Eastern Atlantic rim [EAR]) of Morocco (Fig 6). In general, geographic regions with small representative subsamples yielded comparatively low disparities during the Maastrichtian, including the North African Mediterranean Tethys and North American Western Atlantic rim (WAR) (Fig 6). By contrast, intensive sampling of Stevns Klint in Denmark and the Limhamn Quarry in Sweden skewed the Danian-Selandian geographic distribution toward these regions and revealed the inordinate influence of lagerstätten deposits on our global disparity signal (Fig 6). Lastly, the Thanetian showed a return to more geographically widespread sampling across a continuous *trans*-Atlantic belt, spanning the African epicontinental basins and EAR to the EEB and WAR (Fig 6).

Effects of heterodonty on disparity

Application of the monognathic heterodonty model (Tables CC and DD in S1 Text) produced a significant disparity increase across the Maastrichtian–Danian-Selandian
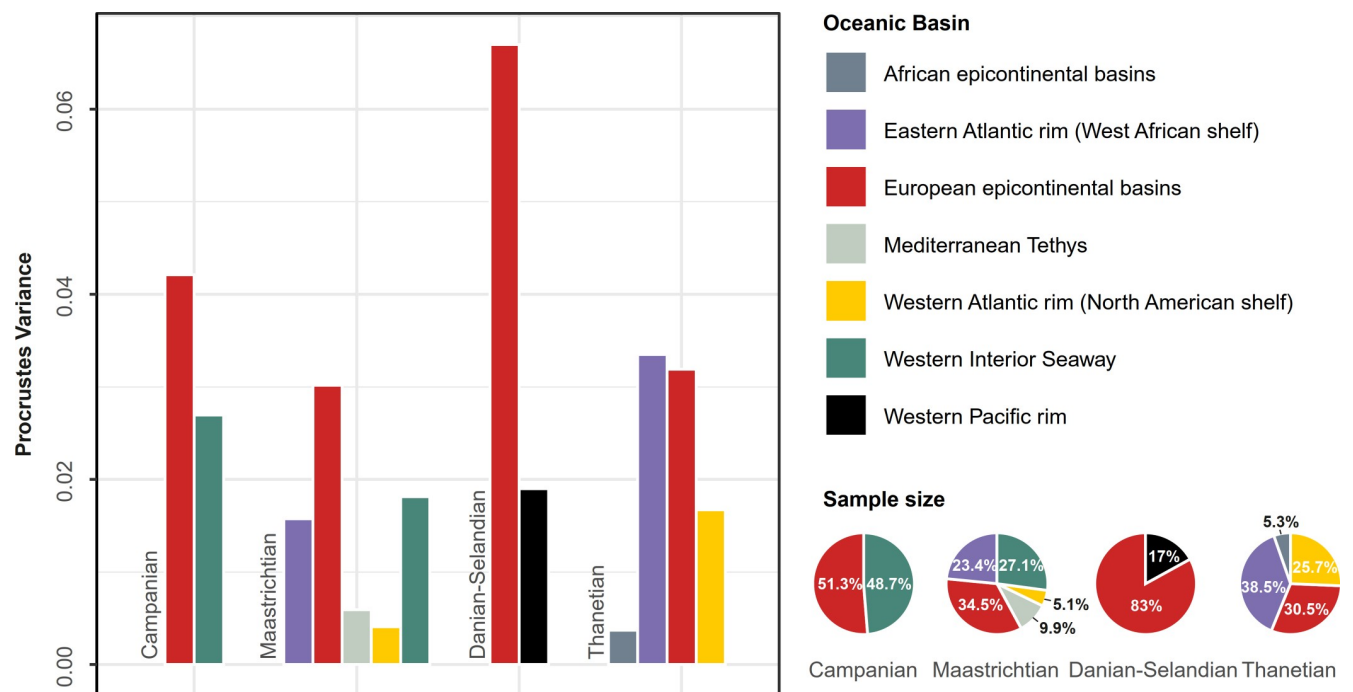

Fig 6. Geographic distribution of disparity. Mesozoic marine depositional basins are based on Wretman and colleagues [75]. Basins with sample sizes of $N < 10$ were omitted. Pie graphs depict sample proportions. The data used in this analysis can be accessed online at https://doi.org/10.5061/dryad.c866t1g5n.

https://doi.org/10.1371/journal.pbio.3001108.g006

($PV_{Maastrichtian} = 0.066$; $PV_{Danian-Selandian} = 0.082$; $p = 0.032$). The combined monognathic and dignathic heterodonty model similarly indicates a disparity increase from the Campanian to Maastrichtian ($p = 0.016$). However, a dignathic heterodonty and multivariate monognathic*dignathic heterodonty interaction model yields no comparable disparity shifts (Fig N and Tables CC and DD in S1 Text), and additional model comparisons found consistent disparity across the Campanian–Thanetian interval, despite some inflation of absolute values (Fig N in S1 Text).

Global morphospace

Pairwise comparisons along all PCs found significant differences ($F_{4, 1,155} = 8.6269$, $p = 0.001$) in morphospace distribution between time-bins (Fig 7, Table 2). The PC1 distributions are platykurtic (kurtosis < 3) and positively skewed, except during the Thanetian, which was negatively skewed ($g1Thanetian = -0.0336$). Distribution-specific interquartile ranges (IQRs) showed minimal morphospace dispersion along PC2 (Tables EE and FF in S1 Text). A Hartigan dip test for multimodality did not reject a unimodal distribution on PC1 or PC2; however, a significant positive morphospace shift did occur from the Maastrichtian–Danian on PC1 (Fig 7A, Fig O and Tables EE and FF in S1 Text). Notably, there was no corresponding change in modal shape configurations, although a reduction in positively loaded morphospace accompanied shortening of the minimum value ranges (Fig 7A, Fig O in S1 Text).

The average value along PC1 shift positively across the Selandian–Thanetian (Fig 7A). Comparisons between the Campanian–Maastrichtian ($p = 0.025$) and Maastrichtian–Thanetian ($p = 0.013$) likewise yield significant morphospace shifts (Table GG in S1 Text).

The distributions for the Campanian and Danian on PC2 are leptokurtic (high kurtosis > 3), but low kurtosis prevails in the other time-bins (Fig 7B). A positive shift from the Maastrichtian ($g1_{Maastrichtian} = -0.0806$) to Danian ($g1_{Danian} = 0.2833$) (Fig 7B, Table EE in S1 Text) coincided with a loss of negatively loaded tooth morphologies (Fig 7B). Nonetheless, the positively loaded morphologies diminished significantly from the Campanian to the Danian ($p = 0.008$) and Maastrichtian–Danian ($p = 0.015$) (Table GG in S1 Text). A comparable morphospace shift across the K/Pg interval was detected using the 4-age time-binning scheme (Fig O in S1 Text) and incorporated subtle changes in modal shape within the Campanian and Maastrichtian–Danian-Selandian time-bins (Fig O in S1 Text).

Regional morphospace

The Stevns Klint regional subsample reveals no substantial shifts along PC1 or PC2 during the late Maastrichtian to early Danian (Fig 8A and 8B, Table GG in S1 Text). However, a significant positive sub-age shift in mean morphology occurred along PC1 from the late Maastrichtian to middle Danian ($p = 0.005$), as well as between the early and middle Danian ($p = 0.005$) (Fig 8A, Table GG in S1 Text). Both the late Maastrichtian ($g1_{late\ Maastrichtian} = 0.2640$) and early Danian ($g1_{early\ Danian} = 0.2957$) are characterized by positively skewed distributions, but with negative skewing during the middle Danian ($g1_{middle\ Danian} = -0.1614$). An increase in negatively loaded morphologies is associated with the early Danian on PC1 and is further reflected in the modal shape configuration (Fig 8A).

The late Maastrichtian distribution on PC2 is negatively skewed, while the early to middle Danian exhibits positive skewing (Fig 8B, Table GG in S1 Text). Modal shape changes are more pronounced along PC2 (Fig 8B), gradually shifting from negatively to positively loaded values (Fig 8B).
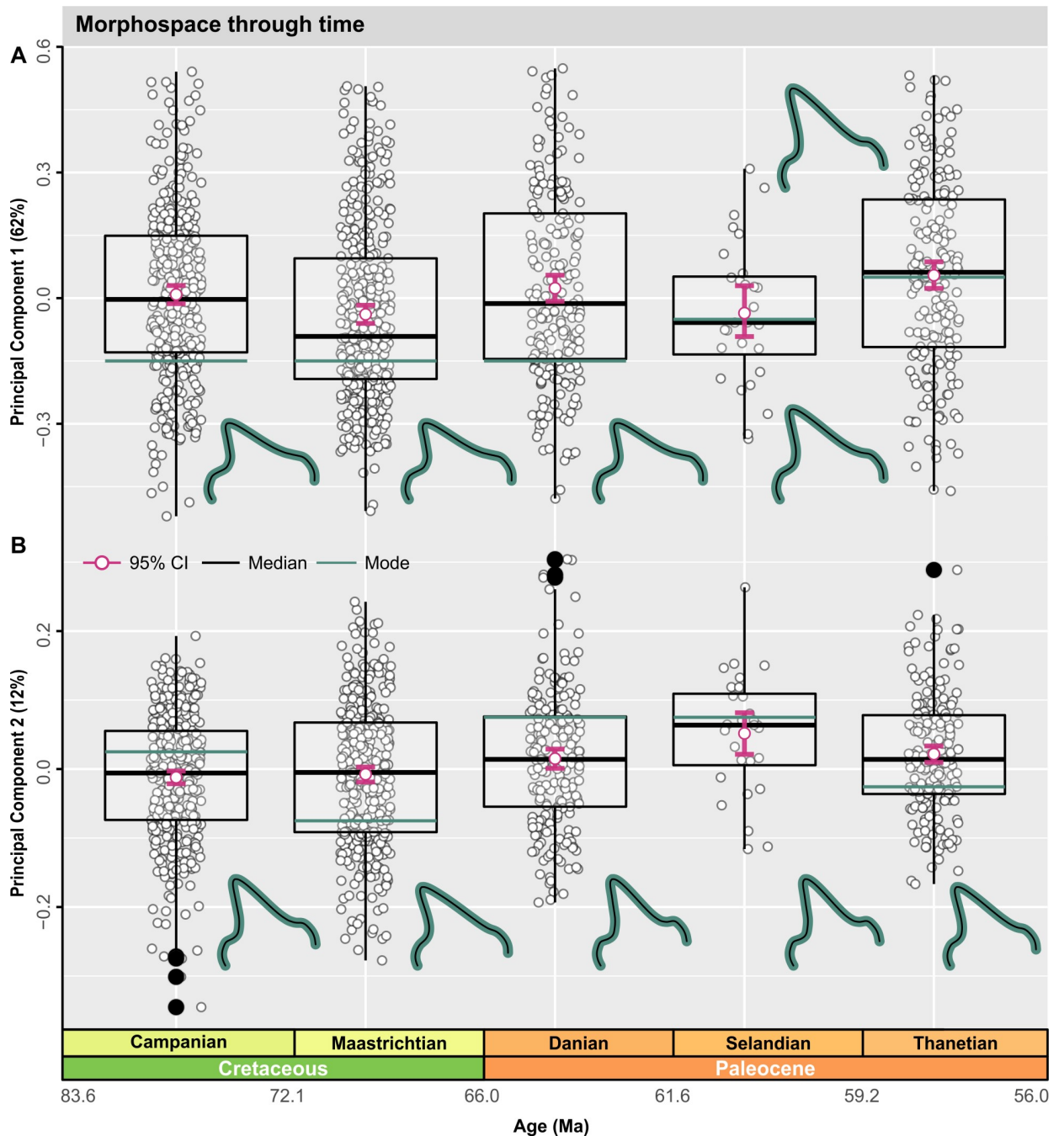
Fig 7. Global morphospace time series. (A, B) Jittered box plots visualizing the distribution of time-bins along PC1 and PC2. Graph depicts patterns of overall shape change using the 5-age time-binning scheme. Measures of central tendency, including the median (black line) and arithmetic mean (pink), are shown with computed 95% nonparametric bootstrap confidence intervals and potential outliers (closed black points). TPS grids indicate changes in modal value (green line) between time-bins. The data used in this analysis can be accessed online at https://doi.org/10.5061/dryad.c866t1g5n. Ma, million years; TPS, thin plate spline.

https://doi.org/10.1371/journal.pbio.3001108.g007

Superorder-level clade morphospace

Galeomorphs and squalomorphs occupied comparable regions of morphospace on PC1 throughout the entire Maastrichtian–Thanetian interval (Fig 9A); although, some differences were evident in their mean and median values. On average, galeomorphs are characterized by

Table 2. Nonparametric analysis of variance based on RRPP for all PCs. Coefficient estimation via OLS. Type I (sequential) sums of squares were used to calculate sums of squares and cross-products matrices. Effect sizes (Z) based on F distribution.

	d.f.	SS	MS	R^2	F	Z	Pr(>F)
Selachimorpha							
~ interaction (global 5-bin)	4	2.625	0.65621	0.02911	8.6269	5.0104	**0.001****
~ interaction (global 4-bin)	3	2.219	0.73957	0.0234	9.5354	4.9451	**0.001****
~ interaction (regional 3-bin)	2	0.840	0.41999	0.06043	4.8235	2.8145	**0.002****
Galeomorphii (Synechodontiformes included)							
~ interaction (global 4-bin)	3	2.254	0.75136	0.02966	10.587	5.0617	**0.001****
~ interaction (regional 3-bin)	2	0.7811	0.39053	0.07727	4.7316	2.796	**0.003****
Squalomorphii							
~ interaction (global 4-bin)	3	0.9088	0.302947	0.07875	4.3028	3.8612	**0.001****
~ interaction (regional 3-bin)	2	0.30381	0.151907	0.12846	2.5058	1.9687	**0.015***

d.f., degrees of freedom; F statistics, F value by permutation; MS, mean squares; OLS, ordinary least squares; RRPP, residual randomization permutation procedure; R^2, coefficient of determination; SS, sequential sums of squares; Z, effect size.

p-Values are based on 999 permutations.

https://doi.org/10.1371/journal.pbio.3001108.t002

tall and narrow teeth, whereas squalomorph teeth are typically low crowned. The most pronounced shift on PC1 is a reduction in negative values among galeomorphs at the K/Pg boundary (Fig 9A) and mirrored on PC3 and PC4 (Table HH in S1 Text). Squalomorphs likewise exhibited a significant positive shift on PC2 ($p = 0.016$) from the Maastrichtian–Danian-Selandian (Fig 9A and 9B, Table II in S1 Text).

Order-level clade morphospace

Lamniforms displayed a significant positive shift in mean morphology along PC1 from the Maastrichtian–Danian-Selandian ($p = 0.002$) (Fig 10A, Table JJ in S1 Text); this is concurrent with an overall positive to negative shift in their distribution ($g1_{Maastrichitan} = 0.5035$; $g1_{Danian-Selandian} = -0.3193$). The frequency of negatively loaded PC1 morphologies is otherwise reduced during the Thanetian and is significantly different from both the Campanian ($p = 0.002$) and Maastrichtian ($p = 0.002$).

Carcharhiniforms maintained stable morphospace occupation along PC1, but their distribution visibly contracted during the K/Pg transition. This is evidenced by a significant negative shift from the Campanian–Danian-Selandian time-bins ($p = 0.024$) and an overall gradual reduction in positive PC1 values (Fig 10A, Table KK in S1 Text).

Heterodontiforms, orectolobiforms, hexanchiforms, squaliforms, squatiniforms, and †synechodontiforms all produce no significant deviations along PC1 across the Campanian–Thanetian interval (Fig 10A, Tables LL to QQ in S1 Text).

Lamniforms exhibited a significant ($p = 0.004$) depletion of negative values from the Maastrichtian–Danian-Selandian on PC2 (Fig 10B). Pairwise comparisons also recovered a significant difference between the Campanian and the Danian–Selandian ($p = 0.004$). By contrast, carcharhiniforms showed no major changes along PC2, except for a slight increase in positive skewness from the Danian-Selandian–Thanetian; this might imply an exploration of new morphospace (Fig 10B). We additionally detected significant differences between the Campanian and Danian-Selandian ($p = 0.031$) and between the Campanian and Thanetian ($p = 0.007$), although this signal reduced after FDR adjustment of the *p*-values (Table KK in S1 Text).

No shifts were recorded for heterodontiforms or orectolobiforms on PC2 (Fig 10B). Yet, these clades did incline toward positive skewness. Squaliforms, squatiniforms, and
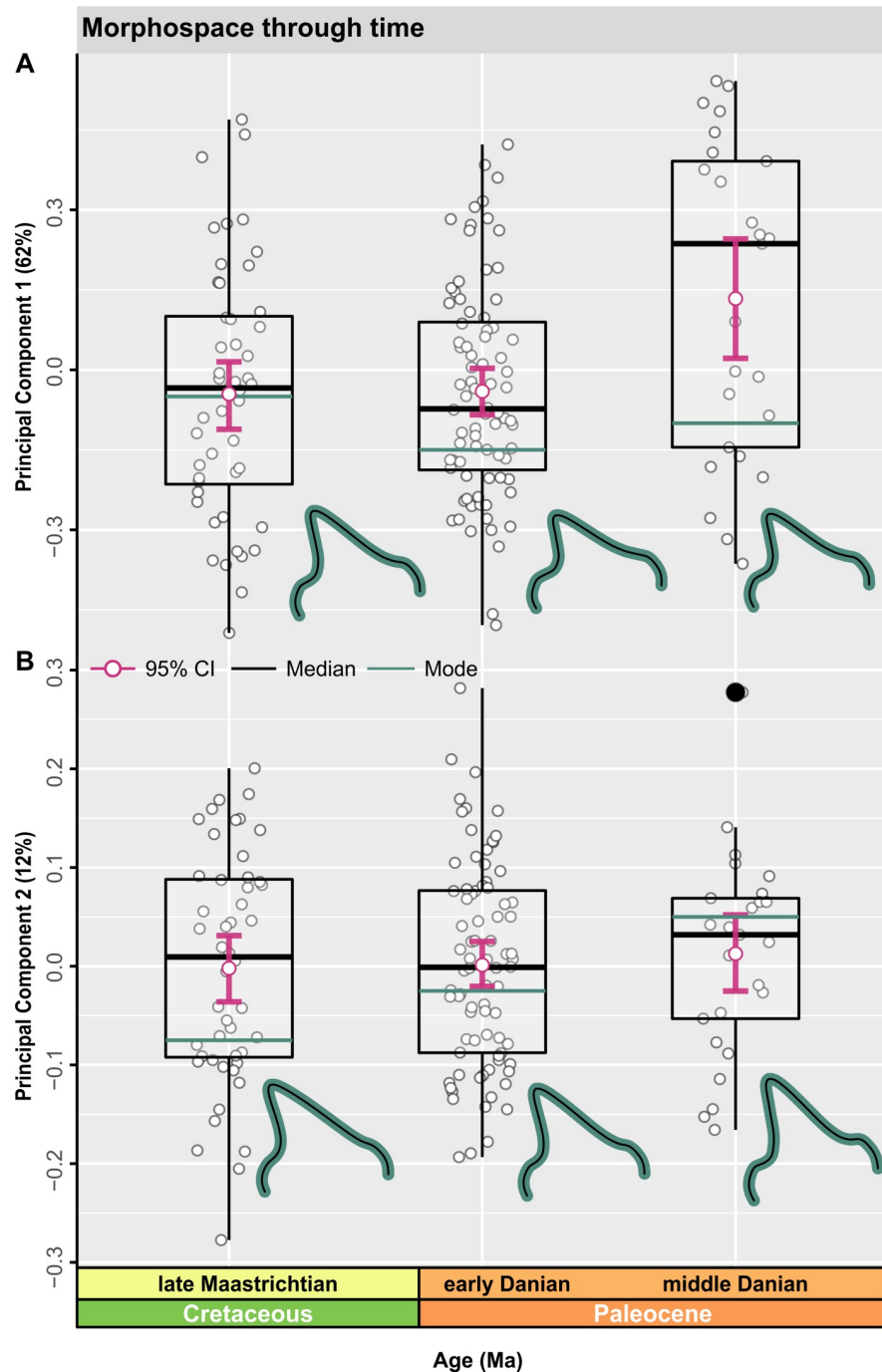
Fig 8. Regional morphospace time series. (A, B) Jittered box plots visualizing the distribution of time-bins along PC1 and PC2 (*n* = 153). Measures of central tendency, including the median (black line) and arithmetic mean (pink), are shown with computed 95% nonparametric bootstrap confidence intervals and potential outliers (closed black points). TPS grids indicate changes in modal value (green line) between time-bins. The data used in this analysis can be accessed online at https://doi.org/10.5061/dryad.c866t1g5n. Ma, million years; TPS, thin plate spline.

https://doi.org/10.1371/journal.pbio.3001108.g008

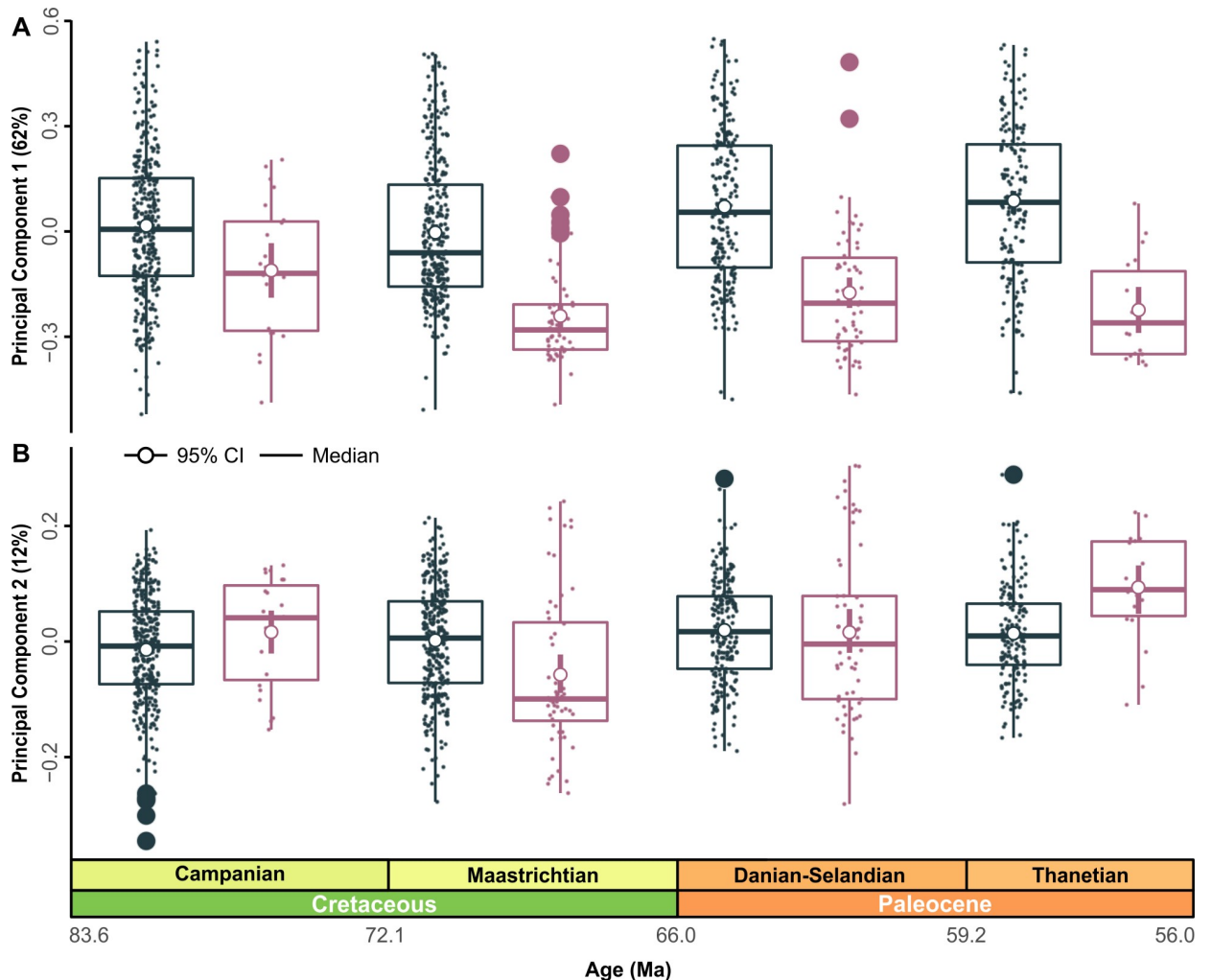**Fig 9. Superorder-level clade morphospace using the global 4-age time-binning scheme. (A–D)** Jittered grouped box plots visualizing the distribution of time-bins along PC1 and PC2. Graph depicts patterns of overall shape change using the 4-age time-binning scheme. Measures of central tendency, including the median and arithmetic mean, are shown with computed 95% nonparametric bootstrap confidence intervals and potential outliers (closed black points). The data used in this analysis can be accessed online at https://doi.org/10.5061/dryad.c866t1g5n. MA, million years.

https://doi.org/10.1371/journal.pbio.3001108.g009

†synechodontiforms likewise experienced no significant changes along PC2 (Tables OO to QQ in S1 Text).

Discussion

Disparity dynamics across the K/Pg boundary

Fundamentally, our results indicate that the global dental disparity of selachimorphs was largely stable across the end-Cretaceous mass extinction, even though some aspects of variance can be attributed to heterodonty (see Fig 2, Fig N and Table CC in S1 Text). Notably, this static disparity concurs with previous analyses of selachimorph disparity [21] and relative abundance patterns in the elasmobranch fossil record [17]. Conversely, diversity-based assessments advocate up to an approximately 50% species loss among selachimorphs over the same time interval [18,19,76].
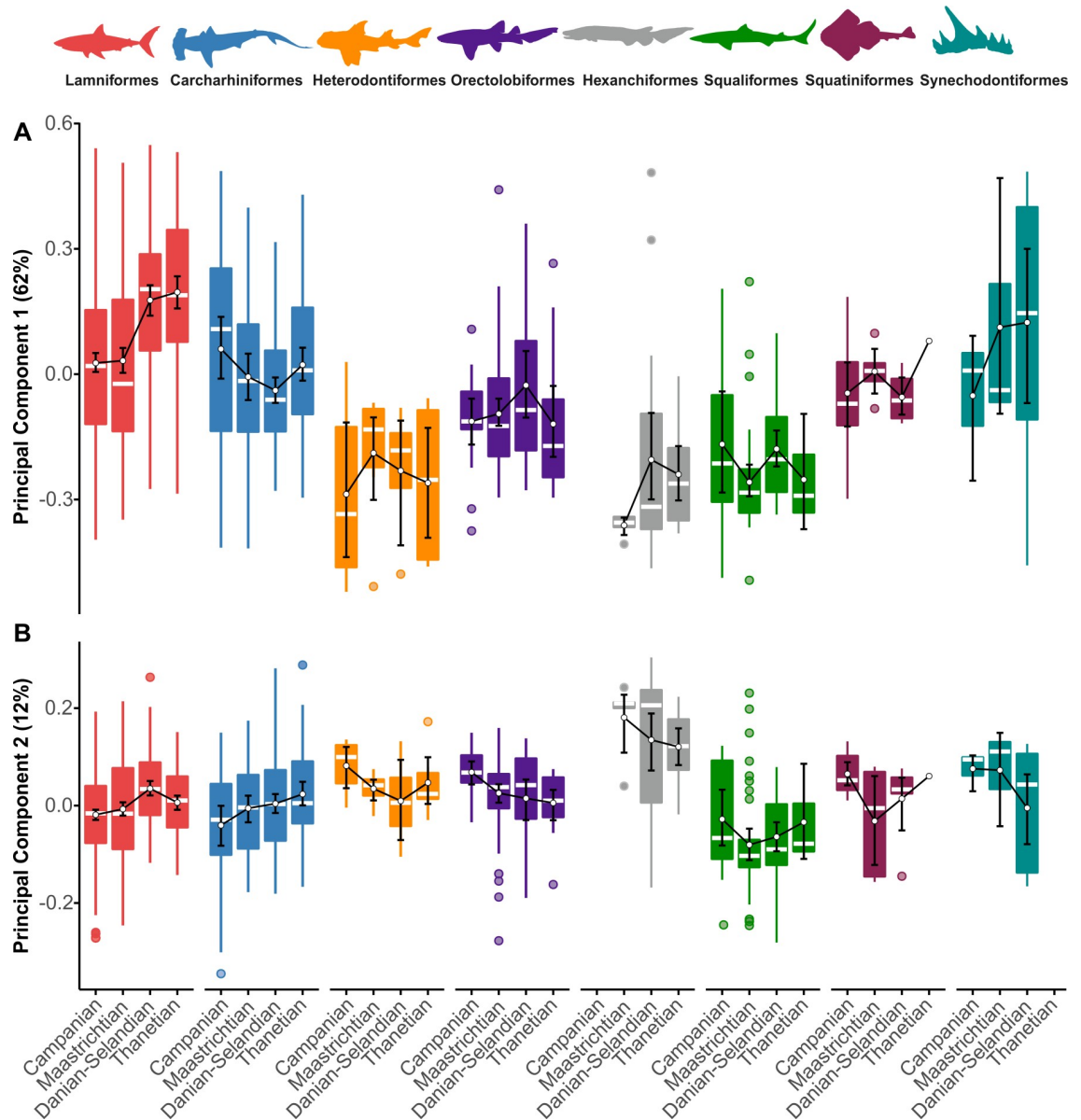
Fig 10. Order-level clade morphospace using the 4-age time-binning scheme. (A, B) Patterns along PC1 and PC2. Sampling was insufficient to estimate reliable disparity for Echinorhiniformes. Measures of central tendency, including the median and arithmetic mean, are shown with computed 95% nonparametric bootstrap confidence intervals and potential outliers. Silhouette graphics created by MB and Julius Csotonyi (https://csotonyi.com/). The data used in this analysis can be accessed online at https://doi.org/10.5061/dryad.c866t1g5n.

https://doi.org/10.1371/journal.pbio.3001108.g010

Taxic decline [18] with no apparent ecological change is expected for a "nonselective" extinction model [77]. Yet, lamniforms as a dominant group did undergo a "selective" extinction of Cretaceous anacoracids [18,21,25], followed by the radiation of odontaspidids in the Paleocene (Fig 10A and 10B). Selective extinction among lamniforms is documented here through the loss of triangular, blade-like tooth morphologies typical of anacoracids versus the subsequent expansion of apicobasally tall, laterally cusped odontaspidid dental morphospace (Fig 10A and 10B). Such a transition would equate to a "shift" extinction model [21] and coincides with the ecological diversification of carcharhiniforms [21], which additionally invaded

mesiodistally broad, low-crowned dental morphospace during the Paleocene (Fig 10A and 10B).

By comparison, squalomorphs were unaffected by the end-Cretaceous mass extinction, although a minor diversity decline is recognized among squalids [18]. We suggest that this group experienced a "nonselective" extinction [77], but with the caveat that their fossil record is poorly sampled (Table A in S1 Text) and should be interpreted cautiously.

Moreover, we emphasize that the proliferation of apicobasally tall dental morphotypes in selachimorphs during the Paleocene does not evince an ecological turnover, unlike the appearance of novel dental grades [78] among coeval actinopterygians [17,20,79–82]. Rather, we propose that while selachimorphs withstood the end-Cretaceous mass extinction, they did suffer sufficient disturbance to trigger a compositional transformation in the morphology of their constituent clades [21,78]—an effect that is best illustrated by the documented fossil histories of lamniforms and carcharhiniforms [21].

Regional versus global extinction dynamics

Adolfssen and Ward [65] reported a 33% decline in chondrichthyan species richness across the K/Pg boundary based on fossils from Stevns Klint. Notably, this is substantially less than both the approximately 96% species loss calculated from K/Pg boundary deposits in Morocco [83] and the approximately 84% estimate derived from global sampling [18]. Stevns Klint preserves a succession of largely endemic Boreal assemblages [65], yet their static dental disparity is indistinguishable from that of the global sample (Fig 2). Nonetheless, we recognize a minor disparity increase (Fig 2) from the early to middle Danian that, although impacted by sampling as evident from rarefaction, corresponds with alterations in absolute disparity values among galeomorphs (Fig 3A). This slight increase, if real, suggests a region-specific postextinction recovery in the early Paleocene.

A more marked geographic transition occurs in regional sampling "hotspots" (Fig 6), which shift from the WIB of North America during the Campanian and Maastrichtian, to the Scandinavian epeiric basins of Denmark and Sweden by the Danian, and, finally, to the Mediterranean Tethys and Atlantic shelf margins of North Africa and Morocco by the Thanetian. While these results undoubtedly capture preservational biases [84], they correlate with the changing depositional contexts of epicontinental environments across the K/Pg time frame. For example, the late Maastrichtian Western Interior Seaway regression [85] coincides with a regional disparity decline in North America, followed by disparity peaks in the transgressive Tethyan peripheries of Europe and North Africa during the Paleocene. Therefore, we suggest that, like other post-mass extinction marine ecosystems [86–88], the recovery of selachimorphs after the K/Pg event might have been geographically localized and centered on epeiric refugia [65] that provided high-productivity habitats conducive to rediversification.

Ecological implications

The end-Cretaceous mass extinction disproportionately affected larger-bodied lamniforms [18,19,21,25]. Body size is also implicated in the extinction of coeval marine reptiles, including mosasaurid lizards and plesiosaurians [89–91]. However, unlike these aquatic tetrapods, Cretaceous lamniform apex predators were supplanted by equally large-bodied hexanchiforms in some earliest Paleocene ecosystems [92]. This accords with our morphospace overlap of anacoracids and hexanchids (Fig P in S1 Text) and is further compatible with some modern shark communities, in which the hexanchid, *Notorynchus cepedianus*, is known to invade apex predator niches once vacated by the lamnid, *Carcharodon carcharias* [93]. Unfortunately, shark body size is difficult to estimate accurately from fossil shark teeth [94,95], and the paleoecology

of Cretaceous anacoracids and hexanchids is poorly understood. Irrespectively, the persistence of larger-bodied selachimorphs across the K/Pg boundary infers size-based niche continuity, a pattern consistent with static dental disparity (this study and [21]), and, thus, the likelihood that other drivers, including diet, habitat preference, and reproductive strategy [96], were influential in selecting for selachimorph extinction susceptibility. Indeed, the Paleocene radiation of piscivorous odontaspidids, triakids, and scyliorhinids coincided with the diversification of teleosts as an emerging food resource [17]. Correspondingly, we posit that feeding "specialization" might have been key to selective lineage loss [21], as well as the differential survival of more adaptable selachimorph "generalist" predators in the end-Cretaceous mass extinction aftermath.

Conclusions

Understanding the dynamics of shark evolution across the end-Cretaceous mass extinction event [18,19,21,22,76] has lagged analytically behind assessments of other marine vertebrate groups, such as teleost fishes [17,20,79–82] and aquatic reptiles [90,91,97,98]. Consequently, we present the first multiclade geometric morphometric evaluation of selachimorph disparity based on their extremely abundant dental fossil record. Our principal discovery of overall static disparity indicates that selachimorphs experienced no demonstrable preextinction decline or eco-morphological turnover as postulated for other vertebrate groups [89,90,99,100]. Nevertheless, the dominant Cretaceous anacoracids suffered a selective extinction, captured here by the loss of triangular, blade-like tooth morphologies traditionally associated with apex predator lifestyles (e.g., feeding on larger-bodied aquatic tetrapods [21]). Furthermore, we show that these extinctions are recognizable on both global and regional scales, although geographic shifts in disparity sampling "hotspots" could implicate changing epeiric habitat availability as another delimiting factor.

From a postextinction perspective, while anacoracids disappeared, other lamniform and carcharhiniform groups ecologically proliferated during the Paleocene. Most notably, this affected odontaspidids, triakids, and scyliorhinids, which are characterized by apicobasally tall, laterally cusped teeth. We interpret this as an extinction-mediated ecological "shift" involving significant changes in dental morphology without substantial modifications to selachimorph overall disparity [21]. Coincidentally, the Paleocene diversification of teleosts offers a potential driver, coupled with the dietary adaptability of selachimorphs as opportunistic "generalist" predators capable of exploiting emergent food resources.

Finally, our analyses underscore the utility of morphospace-disparity analyses to complement traditional taxonomy-based assessments of selachimorph diversity [101,102]. We advocate for similar approaches in future assessments of shark evolution but call attention to heterodonty and differential spatiotemporal sampling as sources of variation that likely mask much of the last 250 Ma of selachimorph eco-morphological evolution.

Supporting information

S1 Text. Supplementary Methods and Results. Supplementary Tables: Tables A–VV. Supplementary Figures: Figs A–DD.
(DOCX)

S1 Data. Global occurrence database.
(XLSX)

S2 Data. 2D-landmark coordinate data.
(TPS)

S3 Data. Sliders file.
(TXT)

S4 Data. Measurement error landmark coordinate data.
(TPS)

S5 Data. Annotated R markdown file.
(PDF)

S6 Data. ReadMe file.
(TXT)

S1 Code. R markdown file containing reproducible R code for running geometric morphometric and statistical analyses of shark dental morphology.
(RMD)

S2 Code. R function used to compute a backtransform morphospace.
(R)

S3 Code. R function used to compute confidence and prediction intervals of the mean, based on a numeric vector.
(R)

S4 Code. R function used to compute univariate descriptive statistics.
(R)

S5 Code. R function used to compute and plot minimum convex hulls for a series of specified points.
(R)

S6 Code. R function used to compute Procrustes variance, bootstrapping, and rarefaction for GPA-aligned data.
(R)

S7 Code. R function used to generate evenly spaced points from point matrix.
(R)

Acknowledgments

Author Contributions

Conceptualization: Mohamad Bazzi, Nicolás E. Campione, Per E. Ahlberg, Henning Blom, Benjamin P. Kear.

Data curation: Mohamad Bazzi.

Formal analysis: Mohamad Bazzi.

Funding acquisition: Mohamad Bazzi, Nicolás E. Campione, Per E. Ahlberg, Benjamin P. Kear.

Investigation: Mohamad Bazzi.

Methodology: Mohamad Bazzi, Nicolás E. Campione.

Supervision: Nicolás E. Campione, Per E. Ahlberg, Henning Blom, Benjamin P. Kear.

Validation: Mohamad Bazzi, Benjamin P. Kear.

Visualization: Mohamad Bazzi.

Writing – original draft: Mohamad Bazzi, Benjamin P. Kear.

Writing – review & editing: Mohamad Bazzi, Nicolás E. Campione, Per E. Ahlberg, Benjamin P. Kear.

References

1. Sepkoski JJ, Bambach RK, Raup DM, Valentine JM. Phanerozoic marine diversity and the fossil record. Nature. 1981:435–437. https://doi.org/10.1038/293435a0

2. Benton MJ. Diversification and extinction in the history of life. Science. 1995; 268:52–8. https://doi.org/10.1126/science.7701342 PMID: 7701342

3. Benton MJ. Exploring macroevolution using modern and fossil data. Proc R Soc B Biol Sci. 2015;282. https://doi.org/10.1098/rspb.2015.0569 PMID: 26063844

4. Raup DM. Taxonomic diversity during the phanerozoic. Science. 1972. https://doi.org/10.1126/science.177.4054.1065 PMID: 17840596

5. Smith AB. Large-scale heterogeneity of the fossil record: Implications for phanerozoic biodiversity studies. Philos Trans R Soc B Biol Sci. 2001. https://doi.org/10.1098/rstb.2000.0768 PMID: 11316484

6. Smith AB, McGowan AJ. The shape of the phanerozoic marine palaeodiversity curve: How much can be predicted from the sedimentary rock record of Western Europe? Palaeontology. 2007. https://doi.org/10.1111/j.1475-4983.2007.00693.x

7. Upchurch P, Mannion PD, Benson RBJ, Butler RJ, Carrano MT. Geological and anthropogenic controls on the sampling of the terrestrial fossil record: A case study from the dinosauria. Geol Soc Spec Publ. 2011. https://doi.org/10.1144/SP358.14

8. Cappetta H. Handbook of Paleoichthyology Volume 3E: Chondrichthyes Mesozoic and Cenozoic Elasmobranchii: Teeth. Munich, Germany: Verlag Dr. Friedrich Pfeil; 2012.

9. Guinot G, Adnet S, Shimada K, Underwood CJ, Siversson M, Ward DJ, et al. On the need of providing tooth morphology in descriptions of extant elasmobranch species. Zootaxa. 2018. https://doi.org/10.11646/zootaxa.4461.1.8 PMID: 30314100

10. Weigmann S. Annotated checklist of the living sharks, batoids and chimaeras (Chondrichthyes) of the world, with a focus on biogeographical diversity. J Fish Biol. 2016. https://doi.org/10.1111/jfb.12874 PMID: 26860638

11. Stein RW, Mull CG, Kuhn TS, Aschliman NC, Davidson LNK, Joy JB, et al. Global priorities for conserving the evolutionary history of sharks, rays and chimaeras. Nat Ecol Evol. 2018; 2:288–98. https://doi.org/10.1038/s41559-017-0448-4 PMID: 29348644

12. Dulvy NK, Fowler SL, Musick JA, Cavanagh RD, Kyne PM, Harrison LR, et al. Extinction risk and conservation of the world's sharks and rays. eLife. 2014. https://doi.org/10.7554/eLife.00590 PMID: 24448405

13. Ferretti F, Worm B, Britten GL, Heithaus MR, Lotze HK. Patterns and ecosystem consequences of shark declines in the ocean. Ecol Lett. 2010. https://doi.org/10.1111/j.1461-0248.2010.01489.x PMID: 20528897

14. Queiroz N, Humphries NE, Couto A, Vedor M, da Costa I, Sequeira AMM, et al. Global spatial risk assessment of sharks under the footprint of fisheries. Nature. 2019. https://doi.org/10.1038/s41586-019-1444-4 PMID: 31340216

15. Roff G, Brown CJ, Priest MA, Mumby PJ. Decline of coastal apex shark populations over the past half century. Commun Biol. 2018. https://doi.org/10.1038/s42003-018-0233-1 PMID: 30564744

16. Pacoureau N, Rigby CL, Kyne PM, Sherley RB, Winker H, Carlson JK, et al. Half a century of global decline in oceanic sharks and rays. Nature. 2021: 589. https://doi.org/10.1038/s41586-020-03173-9 PMID: 33505035

17. Sibert EC, Norris RD. New age of fishes initiated by the Cretaceous-Paleogene mass extinction. Proc Natl Acad Sci U S A. 2015; 112:8537–42. https://doi.org/10.1073/pnas.1504985112 PMID: 26124114

18. Kriwet J, Benton MJ. Neoselachian (Chondrichthyes, Elasmobranchii) diversity across the Cretaceous–Tertiary boundary. Palaeogeogr Palaeoclimatol Palaeoecol. 2004. https://doi.org/10.1016/j.palaeo.2004.02.049

19. Guinot G, Cavin L. 'Fish' (Actinopterygii and Elasmobranchii) diversification patterns through deep time. Biol Rev. 2016; 91:950–81. https://doi.org/10.1111/brv.12203 PMID: 26105527

20. Sibert E, Norris R, Cuevas J, Graves L. Eighty-five million years of pacific ocean gyre ecosystem structure: Long-term stability marked by punctuated change. Proc R Soc B Biol Sci. 2016. https://doi.org/10.1098/rspb.2016.0189 PMID: 27194702

21. Bazzi M, Kear BP, Blom H, Ahlberg PE, Campione NE. Static Dental Disparity and Morphological Turnover in Sharks across the End-Cretaceous Mass Extinction. Curr Biol. 2018. https://doi.org/10.1016/j.cub.2018.05.093 PMID: 30078565

22. Belben RA, Underwood CJ, Johanson Z, Twitchett RJ. Ecological impact of the end-Cretaceous extinction on lamniform sharks. PLoS ONE. 2017. https://doi.org/10.1371/journal.pone.0178294 PMID: 28591222

23. Ikejiri T, Lu YH, Zhang B. Two-step extinction of Late Cretaceous marine vertebrates in northern Gulf of Mexico prolonged biodiversity loss prior to the Chicxulub impact. Sci Rep. 2020. https://doi.org/10.1038/s41598-020-61089-w PMID: 32144332

24. Miller KG, Sugarman PJ, Browning JV, Kominz MA, Hernández JC, Olsson RK, et al. Late Cretaceous chronology of large, rapid sea-level changes: Glacioeustasy during the greenhouse world. Geology. 2003. https://doi.org/10.1130/0091-7613(2003)031<0585:LCCOLR>2.0.CO;2

25. Friedman M, Sallan LC. Five hundred million years of extinction and recovery: A phanerozoic survey of large-scale diversity patterns in fishes. Palaeontology. 2012; 55:707–42. https://doi.org/10.1111/j.1475-4983.2012.01165.x

26. Claude J. Morphometrics with R. Springer Science & Business Media; 2008. Available from: https://www.researchgate.net/publication/258885233

27. Webster M, Sheets HD. A Practical Introduction to Landmark-Based Geometric Morphometrics. Paleontol Soc Pap. 2010. https://doi.org/10.1017/s1089332600001868

28. Gottfried MD, Rabarison JA. First Mesozoic Gondwanan record of a sawshark (Chondrichthyes, Pristiophoriformes), from the Late Cretaceous of Madagascar. J Vertebr Paleontol. 1997. https://doi.org/10.1080/02724634.1997.10011022

29. De Carvalho MR. Higher-Level Elasmobranch Phylogeny, Basal Squaleans, and Paraphyly. Interrelationships of Fishes. 1996. https://doi.org/10.1016/b978-012670950-6/50004-7

30. Naylor GJ, Caira JN, Jensen K, Rosana K, Straube N, Lakner C. Elasmobranch Phylogeny: A Mitochondrial Estimate Based on 595 Species. Biology of sharks and their relatives. 2012. https://doi.org/10.1080/17451000.2012.745005

31. Ebert DA, Fowler SL, Compagno LJ. Sharks of the World: A Fully Illustrated Guide. Wild Nature Press; 2013.

32. Maisey JG. Cranial Morphology of the Fossil Elasmobranch Synechodus dubrisiensis. Am Museum Novit. 1985.

33. Klug S, Kriwet J, BÖttcher R, Schweigert G, Dietl G. Skeletal anatomy of the extinct shark Paraorthacodus jurensis (Chondrichthyes; Palaeospinacidae), with comments on synechodontiform and palaeospinacid monophyly. Zool J Linnean Soc. 2009. https://doi.org/10.1111/j.1096-3642.2009.00534.x

34. Klug S. Monophyly, phylogeny and systematic position of the † synechodontiformes (Chondrichthyes, Neoselachii). Zool Scr. 2010. https://doi.org/10.1111/j.1463-6409.2009.00399.x

35. Maisey JG. What is an "elasmobranch"? The impact of palaeontology in understanding elasmobranch phylogeny and evolution. J Fish Biol. 2012; 80:918–51. https://doi.org/10.1111/j.1095-8649.2012.03245.x PMID: 22497368

36. Cohen KM, Finney SC, Gibbard PL, Fan JX. The ICS international chronostratigraphic chart. Episodes. 2013. https://doi.org/10.18814/epiiugs/2013/v36i3/002

37. Bookstein FL. Morphometric Tools for Landmark Data. Cambridge University Press; 1991. https://doi.org/10.1017/cbo9780511573064

38. Dryden IL, Mardia KV. Statistical Shape Analysis, with Applications in R: Second Edition. John Wiley & Sons Ltd.; 2016. https://doi.org/10.1002/9781119072492

39. Slice DE. Geometric Morphometrics. Annu Rev Anthropol. 2007. https://doi.org/10.1146/annurev.anthro.34.081804.120613

40. Adams DC, Rohlf FJ, Slice DE. Geometric morphometrics: Ten years of progress following the 'revolution. Ital J Zool. 2004. https://doi.org/10.1080/11250000409356545

41. Zelditch M, Swiderski D, Sheets H. Geometric Morphometrics for Biologists. 2012. https://doi.org/10.1016/C2010-0-66209-2

42. Mitteroecker P, Gunz P. Advances in Geometric morphometrics. Evol Biol. 2009. https://doi.org/10.1007/s11692-009-9055-x

43. Rohlf FJ. tpsDig. 2016. Available from: http//life.bio.sunysb.edu/morph/. https://doi.org/10.1093/jac/dkf017

44. Team RC. R: A Language and Environment for Statistical Computing. Vienna, Austria. 2019.

45. Moyer JK, Bemis WE. Shark teeth as edged weapons: serrated teeth of three species of selachians. Zoology. 2017; 120:101–9. https://doi.org/10.1016/j.zool.2016.05.007 PMID: 27353190

46. Arnqvist G, Mårtensson T. Measurement error in geometric morphometrics: Empirical strategies to assess and reduce its impact on measures of shape. Acta Zool Acad Sci Hungaricae. 1998.

47. Yezerinac SM, Lougheed SC, Handford P. Measurement error and morphometric studies: Statistical power and observer experience. Syst Biol. 1992. https://doi.org/10.1093/sysbio/41.4.471

48. Adams D, Collyer M, Kaliontzopoulou A, Sherratt E. Geomorph: Software for geometric morphometric analyses. R package version 3.2.1. 2020. Available from: https://cran.r-project.org/package=geomorph

49. Rohlf FJ, Slice D. Extensions of the procrustes method for the optimal superimposition of landmarks. Syst Zool. 1990. https://doi.org/10.2307/2992207

50. Bookstein FL. Landmark methods for forms without landmarks: Morphometrics of group differences in outline shape. Med Image Anal. 1997. https://doi.org/10.1016/s1361-8415(97)85012-8 PMID: 9873908

51. Gunz P, Mitteroecker P, Bookstein FL. Semilandmarks in Three Dimensions. Modern Morphometrics in Physical Anthropology. 2006. https://doi.org/10.1007/0-387-27614-9_3

52. Bonhomme V, Picq S, Gaucherel C, Claude J. Momocs: Outline analysis using R. J Stat Softw. 2014; 56:1–24. https://doi.org/10.18637/jss.v056.i13

53. MacLeod N. Form & shape models. Palaeontol Newsl. 2009; 18:1–11.

54. Olsen AM. Feeding ecology is the primary driver of beak shape diversification in waterfowl. Funct Ecol. 2017; 31:1985–95. https://doi.org/10.1111/1365-2435.12890

55. Collyer ML, Adams DC. RRPP: An r package for fitting linear models to high-dimensional data using residual randomization. Methods Ecol Evol. 2018. https://doi.org/10.1111/2041-210X.13029

56. Wickham H. ggplot2 Elegant Graphics for Data Analysis. Journal of the Royal Statistical Society: Series A (Statistics in Society). 2016. https://doi.org/10.1007/978-3-319-24277-4

57. Bazzi M. Data from: Tooth morphology elucidates shark evolution across the end-Cretaceous mass extinction. Dryad Repos. 2021. https://doi.org/10.5061/dryad.c866t1g5n

58. Korkmaz S, Goksuluk D, Zararsiz G. MVN: An R package for assessing multivariate normality. R J. 2014. https://doi.org/10.32614/rj-2014-031

59. Zelditch ML, Sheets HD, Fink WL. The ontogenetic dynamics of shape disparity. Paleobiology. 2003. https://doi.org/10.1666/0094-8373(2003)029<0139:todosd>2.0.co;2

60. Foote M. Contributions of individual taxa to overall morphological disparity. Paleobiology. 1993. https://doi.org/10.1017/S0094837300014056

61. Benjamini Y, Hochberg Y. Controlling the False Discovery Rate: A Practical and Powerful Approach to Multiple Testing. J R Stat Soc Ser B. 1995. https://doi.org/10.1111/j.2517-6161.1995.tb02031.x

62. Alroy J. Geographical, environmental and intrinsic biotic controls on Phanerozoic marine diversification. Palaeontology. 2010. https://doi.org/10.1111/j.1475-4983.2010.01011.x

63. Close RA, Benson RBJ, Upchurch P, Butler RJ. Controlling for the species-area effect supports constrained long-term Mesozoic terrestrial vertebrate diversification. Nat Commun. 2017. https://doi.org/10.1038/ncomms15381 PMID: 28530240

64. Mannion PD, Chiarenza AA, Godoy PL, Cheah YN. Spatiotemporal sampling patterns in the 230 million year fossil record of terrestrial crocodylomorphs and their impact on diversity. Palaeontology. 2019. https://doi.org/10.1111/pala.12445 PMID: 32025055

65. Adolfssen JS, Ward DJ. Crossing the boundary: An elasmobranch fauna from Stevns Klint. Denmark Palaeontology. 2014. https://doi.org/10.1111/pala.12079

66. Adolfssen JS, Ward DJ. Neoselachians from the Danian (early Paleocene) of Denmark. Acta Palaeontol Pol. 2015. https://doi.org/10.4202/app.2012.0123

67. Alvarez LW, Alvarez W, Asaro F, Michel HV. Extraterrestrial cause for the Cretaceous-Tertiary extinction. Science. 1980. https://doi.org/10.1126/science.208.4448.1095 PMID: 17783054

68. Huber D, Wilga C, Dean M, Ferry L, Gardiner J, Habegger L, et al. Feeding in Cartilaginous Fishes: An Interdisciplinary Synthesis. Springer, Cham; 2019. pp. 231–295. https://doi.org/10.1007/978-3-030-13739-7_8

69. Shimada K. Dental homologies in lamniform sharks (Chondrichthyes: Elasmobranchii). J Morphol. 2002. https://doi.org/10.1002/jmor.1073 PMID: 11746467

70. Cullen JA, Marshall CD. Do sharks exhibit heterodonty by tooth position and over ontogeny? A comparison using elliptic Fourier analysis. J Morphol. 2019; 280:687–700. https://doi.org/10.1002/jmor.20975 PMID: 30861183

71. Tomita T, Miyamoto K, Kawaguchi A, Toda M, Oka SI, Nozu R, et al. Dental ontogeny of a white shark embryo. J Morphol. 2017. https://doi.org/10.1002/jmor.20630 PMID: 27889924

72. Jablonski D. Micro- and macroevolution: Scale and hierarchy in evolutionary biology and paleobiology. Paleobiology. 2000. https://doi.org/10.1666/0094-8373(2000)026<0007:cdappc>2.0.co;2 PMID: 11543303

73. Gerber S. On the Relationship between the Macroevolutionary Trajectories of Morphological Integration and Morphological Disparity. PLoS ONE. 2013. https://doi.org/10.1371/journal.pone.0063913 PMID: 23691115

74. Berio F, Evin A, Goudemand N, Debiais-Thibaud M. The intraspecific diversity of tooth morphology in the large-spotted catshark *Scyliorhinus stellaris*: insights into the ontogenetic cues driving sexual dimorphism. J Anat. 2020. https://doi.org/10.1111/joa.13257 PMID: 32667054

75. Wretman L, Blom H, Kear BP. Resolution of the Early Jurassic actinopterygian fish Pachycormus and a dispersal hypothesis for Pachycormiformes. J Vertebr Paleontol. 2016; 36:e1206022. https://doi.org/10.1080/02724634.2016.1206022

76. Guinot G, Adnet S, Cappetta H. An Analytical Approach for Estimating Fossil Record and Diversification Events in Sharks, Skates and Rays. PLoS ONE. 2012. https://doi.org/10.1371/journal.pone.0044632 PMID: 22957091

77. Foote M. Discordance and concordance between morphological and taxonomic diversity. Paleobiology. 1993. https://doi.org/10.1017/S0094837300015864

78. Sibert E, Friedman M, Hull P, Hunt G, Norris R. Two pulses of morphological diversification in Pacific pelagic fishes following the Cretaceous-Palaeogene mass extinction. Proc R Soc B Biol Sci. 2018. https://doi.org/10.1098/rspb.2018.1194 PMID: 30305432

79. Friedman M. Explosive morphological diversification of spiny-finned teleost fishes in the aftermath of the end-Cretaceous extinction. Proc R Soc B Biol Sci. 2010. https://doi.org/10.1098/rspb.2009.2177 PMID: 20133356

80. Miya M, Friedman M, Satoh TP, Takeshima H, Sado T. Evolutionary Origin of the Scombridae (Tunas and Mackerels): Members of a Paleogene Adaptive Radiation with 14 Other Pelagic Fish Families. PLoS ONE. 2013; 8:73535. https://doi.org/10.1371/journal.pone.0073535 PMID: 24023883

81. Near TJ, Dornburg A, Eytan RI, Keck BP, Smith WL, Kuhn KL, et al. Phylogeny and tempo of diversification in the superradiation of spiny-rayed fishes. Proc Natl Acad Sci U S A. 2013. https://doi.org/10.1073/pnas.1304661110 PMID: 23858462

82. Ribeiro E, Davis AM, Rivero-Vega RA, Ortí G, Betancur R. Post-Cretaceous bursts of evolution along the benthic-pelagic axis in marine fishes. Proc R Soc B Biol Sci. 2018. https://doi.org/10.1098/rspb.2018.2010 PMID: 30963906

83. Noubhani A, Cappetta H. Les Orectolobiformes, Carcharhiniformes et Myliobatiformes (Elasmobranchii, Neoselachii) des Bassins a phosphate du Maroc (Maastrichtien–Lutetien basal): systématique, biostratigraphie, évolution et dynamique des faunes. Palaeo Ichthyol. 1997; 8:327.

84. Jackson JBC, Johnson KG. Measuring past biodiversity. Science. 2001. https://doi.org/10.1126/science.1063789 PMID: 11577222

85. Cochran JK, Landman NH, Turekian KK, Michard A, Schrag DP. Paleoceanography of the Late Cretaceous (Maastrichtian) Western Interior Seaway of North America: Evidence from Sr and O isotopes. Palaeogeogr Palaeoclimatol Palaeoecol. 2003. https://doi.org/10.1016/S0031-0182(02)00642-9

86. Jablonski D. Geographic Variation in the Molluscan Recovery from the End-Cretaceous Extinction. 1998. Available from: http://science.sciencemag.org/ https://doi.org/10.1126/science.279.5355.1327 PMID: 9478887

87. Patzkowsky AZK and ME. Geographic variation in turnover and recovery from the Late Ordovician mass extinction. Paleobiology. 2007; 33: 435–454. Available from: https://pubs.geoscienceworld.org/paleobiol/article-abstract/33/3/435/86456

88. Zatoń M, Niedźwiedzki G, Blom H, Kear BP. Boreal earliest Triassic biotas elucidate globally depauperate hard substrate communities after the end-Permian mass extinction. Sci Rep. 2016; 6:1–10. https://doi.org/10.1038/s41598-016-0001-8 PMID: 28442746

89. Benson RBJ, Butler RJ. Uncovering the diversification history of marine tetrapods: Ecology influences the effect of geological sampling biases. Geol Soc Spec Publ. 2011. https://doi.org/10.1144/SP358.13

90. Martin JE, Vincent P, Tacail T, Khaldoune F, Jourani E, Bardet N, et al. Calcium Isotopic Evidence for Vulnerable Marine Ecosystem Structure Prior to the K/Pg Extinction. Curr Biol. 2017; 27: 1641–1644. e2. https://doi.org/10.1016/j.cub.2017.04.043 PMID: 28552352

91. Bardet N. Extinction Events Among Mesozoic Marine Reptiles. Hist Biol. 1994. https://doi.org/10.1080/10292389409380462

92. Siverson M. Revision of the danian cow sharks, sand tiger sharks, and goblin sharks (hexanchidae, odontaspididae, and mitsukurinidae) from southern Sweden. J Vertebr Paleontol. 1995. https://doi.org/10.1080/02724634.1995.10011203

93. Hammerschlag N, Williams L, Fallows M, Fallows C. Disappearance of white sharks leads to the novel emergence of an allopatric apex predator, the sevengill shark. Sci Rep. 2019. https://doi.org/10.1038/s41598-018-37576-6 PMID: 30760739

94. Shimada K, Becker MA, Griffiths ML. Body, jaw, and dentition lengths of macrophagous lamniform sharks, and body size evolution in Lamniformes with special reference to 'off-the-scale' gigantism of the megatooth shark. Otodus megalodon Hist Biol. 2020. https://doi.org/10.1080/08912963.2020.1812598

95. Perez V, Leder R, Badaut T. Body length estimation of Neogene macrophagous lamniform sharks (Carcharodon and Otodus) derived from associated fossil dentitions. Palaeontol Electron. 2021. https://doi.org/10.26879/1140

96. García VB, Lucifora LO, Myers RA. The importance of habitat and life history to extinction risk in sharks, skates, rays and chimaeras. Proc R Soc B Biol Sci. 2008. https://doi.org/10.1098/rspb.2007.1295 PMID: 17956843

97. Polcyn MJ, Jacobs LL, Araújo R, Schulp AS, Mateus O. Physical drivers of mosasaur evolution. Palaeogeogr Palaeoclimatol Palaeoecol. 2014. https://doi.org/10.1016/j.palaeo.2014.08.015 PMID: 26089574

98. Cleary TJ, Benson RBJ, Holroyd PA, Barrett PM. Tracing the patterns of non-marine turtle richness from the Triassic to the Palaeogene: from origin to global spread. Palaeontology. 2020. https://doi.org/10.1111/pala.12445 PMID: 32025055

99. Field DJ, Bercovici A, Berv JS, Dunn R, Fastovsky DE, Lyson TR, et al. Early Evolution of Modern Birds Structured by Global Forest Collapse at the End-Cretaceous Mass Extinction. Curr Biol. 2018. https://doi.org/10.1016/j.cub.2018.04.062 PMID: 29804807

100. Chiarenza AA, Farnsworth A, Mannion PD, Lunt DJ, Valdes PJ, Morgan JV, et al. Asteroid impact, not volcanism, caused the end-Cretaceous dinosaur extinction. Proc Natl Acad Sci U S A. 2020. https://doi.org/10.1073/pnas.2006087117 PMID: 32601204

101. Hetherington AJ, Sherratt E, Ruta M, Wilkinson M, Deline B, Donoghue PCJ. Do cladistic and morphometric data capture common patterns of morphological disparity? Palaeontology. 2015. https://doi.org/10.1111/pala.12159

102. Brusatte SL, Benton MJ, Ruta M, Lloyd GT. Superiority, competition, and opportunism in the evolutionary radiation of dinosaurs. Science. 2008. https://doi.org/10.1126/science.1161833 PMID: 18787166